QUANTUM CHROMODYNAMICS

A. Pich

Departament de Física Teòrica and IFIC, Universitat de València – CSIC
Dr. Moliner 50, E–46100 Burjassot, València, Spain

Abstract

These lectures provide an overview of Quantum Chromodynamics (QCD), the $SU(3)_C$ gauge theory of the strong interactions. After briefly reviewing the empirical considerations which lead to the introduction of *colour*, the QCD Lagrangian is discussed. The running of the strong coupling and the associated property of *Asymptotic Freedom* are analyzed. Some selected experimental tests and the present knowledge of α_s are summarized. A short description of the QCD flavour symmetries and the *dynamical breaking of chiral symmetry* is also given. A more detailed discussion can be found in standard textbooks [1–4] and recent reviews [5–9].

1.   QUARKS AND COLOUR

A fast look into the Particle Data Tables [10] reveals the richness and variety of the hadronic spectrum. The large number of known mesonic and baryonic states clearly signals the existence of a deeper level of elementary constituents of matter: *quarks* [11]. In fact, the messy hadronic world can be easily understood in terms of a few constituent spin-$\frac{1}{2}$ quark *flavours*:

$Q = +\frac{2}{3}$	u	c	t
$Q = -\frac{1}{3}$	d	s	b

Assuming that mesons are $M \equiv q\bar{q}$ states, while baryons have three quark constituents, $B \equiv qqq$, one can nicely classify the entire hadronic spectrum:

$$\pi^+ = u\bar{d}, \quad K^+ = u\bar{s}, \quad K^0 = d\bar{s}, \quad \pi^0 = (u\bar{u} - d\bar{d})/\sqrt{2} \ \ldots$$

$$D^+ = c\bar{d}, \quad D^0 = c\bar{u}, \quad D_s^+ = c\bar{s} \quad \ldots$$

$$B^+ = u\bar{b}, \quad B^0 = d\bar{b}, \quad B_s^0 = s\bar{b}, \quad B_c^+ = c\bar{b} \ \ldots$$

$$p = uud, \quad n = udd, \quad \Sigma^+ = uus, \quad \Sigma^0 = uds \ \ldots$$

$$\Sigma_c^+ = udc, \quad \Sigma_c^{++} = uuc, \quad \Xi_c^+ = usc, \quad \Xi_c^0 = dsc \ \ldots$$

$$\Xi_{cc}^+ = dcc, \quad \Xi_{cc}^{++} = ucc, \quad \Omega_{cc}^+ = scc \quad \ldots$$

There is a one–to–one correspondence between the observed hadrons and the states predicted by this simple classification; thus, the *Quark Model* appears to be a very useful *Periodic Table of Hadrons*. However, the quark picture faces a problem concerning the Fermi–Dirac statistics of the constituents. Since the fundamental state of a composite system is expected to have $L = 0$, the Δ^{++} baryon ($J = \frac{3}{2}$) corresponds to $u^\uparrow u^\uparrow u^\uparrow$, with the three quark-spins aligned into the same direction ($s_3 = +\frac{1}{2}$) and all relative angular momenta equal to zero. The wave function is symmetric and, therefore, the Δ^{++} state obeys the wrong statistics.

The problem can be solved assuming [12] the existence of a new quantum number, *colour*, such that each species of quark may have $N_C = 3$ different colours: q^α, $\alpha = 1, 2, 3$ (red, yellow, violet). Then one can reinterpret the Δ^{++} as the antisymmetric state

$$\Delta^{++} = \frac{1}{\sqrt{6}} \epsilon^{\alpha\beta\gamma} |u_\alpha^\uparrow u_\beta^\uparrow u_\gamma^\uparrow\rangle \tag{1.1}$$

(notice that at least 3 colours are needed for making an antisymmetric state). In this picture, baryons and mesons are described by the colour-singlet combinations

$$B = \frac{1}{\sqrt{6}} \epsilon^{\alpha\beta\gamma} |q_\alpha q_\beta q_\gamma\rangle , \qquad\qquad M = \frac{1}{\sqrt{3}} \delta^{\alpha\beta} |q_\alpha \bar{q}_\beta\rangle . \tag{1.2}$$

In order to avoid the existence of non-observed extra states with non-zero colour, one needs to further postulate that all asymptotic states are colourless, i.e. singlets under rotations in colour space. This assumption is known as the *confinement hypothesis*, because it implies the non-observability of free quarks: since quarks carry colour they are confined within colour-singlet bound states.

The quark picture is not only a nice mathematical scheme to classify the hadronic world. We have strong experimental evidence of the existence of quarks. Fig. 1 shows a typical $Z \to$ hadrons event, obtained at LEP. Although there are many hadrons in the final state, they appear to be collimated in 2 *jets* of particles, as expected from a two-body decay $Z \to q\bar{q}$, where the $q\bar{q}$ pair has later *hadronized*.

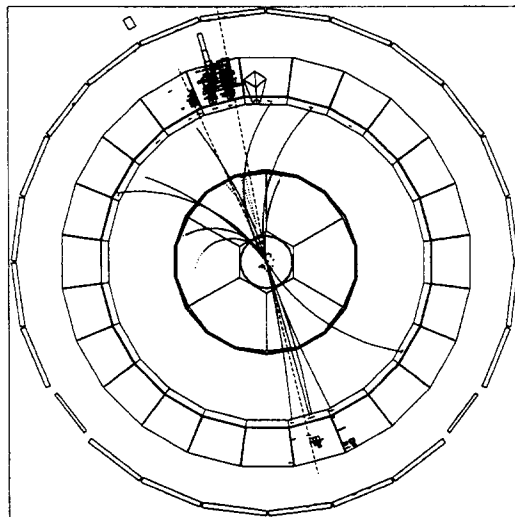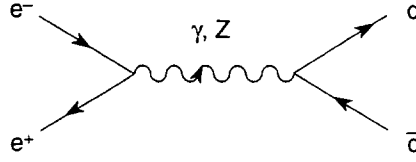Figure 1: Two-jet event from the hadronic decay of a Z boson (DELPHI).

Figure 2: Feynman diagram for $e^+e^- \rightarrow$ hadrons.

1.1 Evidence of colour

A direct test of the colour quantum number can be obtained from the ratio

$$R_{e^+e^-} \equiv \frac{\sigma(e^+e^- \rightarrow \text{hadrons})}{\sigma(e^+e^- \rightarrow \mu^+\mu^-)}. \qquad (1.3)$$

The hadronic production occurs through $e^+e^- \rightarrow \gamma^*, Z^* \rightarrow q\bar{q} \rightarrow$ hadrons. Since quarks are assumed to be confined, the probability to hadronize is just one; therefore, the sum over all possible quarks in the final state will give the total inclusive cross-section into hadrons. At energies well below the Z peak, the cross-section is dominated by the γ-exchange amplitude; the ratio $R_{e^+e^-}$ is then given by the sum of the quark electric charges squared:

$$R_{e^+e^-} \approx N_C \sum_{f=1}^{N_f} Q_f^2 = \begin{cases} \frac{2}{3}N_C = 2\,, & (N_f = 3 \,:\, u,d,s) \\ \frac{10}{9}N_C = \frac{10}{3}\,, & (N_f = 4 \,:\, u,d,s,c) \\ \frac{11}{9}N_C = \frac{11}{3}\,, & (N_f = 5 \,:\, u,d,s,c,b) \end{cases} \qquad (1.4)$$
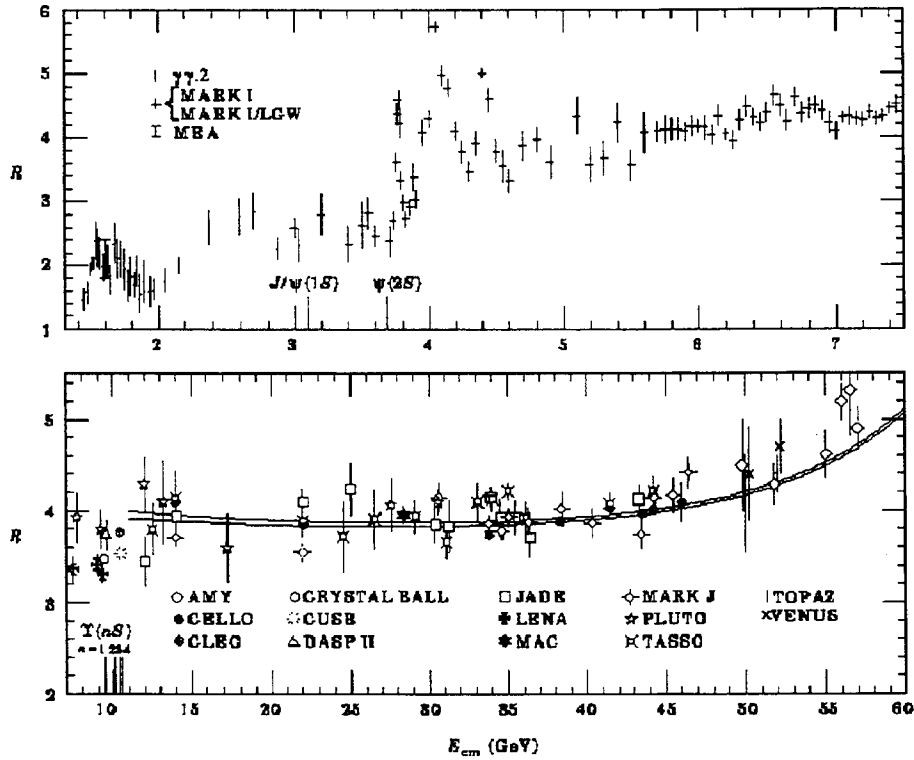

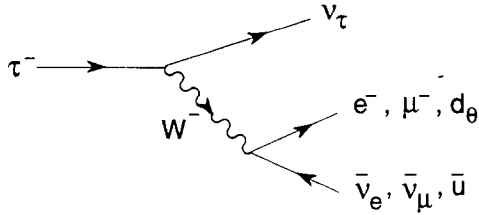Figure 3: Measurements of $R_{e^+e^-}$ [10]. The two continuous curves are QCD fits.

159

Figure 4: τ-decay diagram.

The measured ratio is shown in Fig. 3. Although the simple formula (1.4) cannot explain the complicated structure around the different quark thresholds, it gives the right average value of the cross-section (away from the thresholds), provided that N_C is taken to be three. The agreement is better at larger energies. Notice that strong interactions have not been taken into account; only the confinement hypothesis has been used.

The hadronic decay of the τ lepton provides additional evidence for $N_C = 3$. The decay proceeds through the W-emission diagram shown in Fig. 4. Since the W coupling to the charged current is of universal strength, there are $(2 + N_C)$ equal contributions (if final masses and strong interactions are neglected) to the τ-decay width. Two of them correspond to the leptonic decay modes $\tau^- \to \nu_\tau e^- \bar{\nu}_e$ and $\tau^- \to \nu_\tau \mu^- \bar{\nu}_\mu$, while the other N_C are associated with the possible colours of the quark–antiquark pair in the $\tau^- \to \nu_\tau d_\theta u$ decay mode ($d_\theta \equiv \cos\theta_C d + \sin\theta_C s$). Hence, the branching ratios for the different channels are expected to be approximately:

$$B_{\tau \to l} \equiv Br(\tau^- \to \nu_\tau l^- \bar{\nu}_l) \approx \frac{1}{2 + N_C} = \frac{1}{5} = 20\%, \qquad (1.5)$$

$$R_\tau \equiv \frac{\Gamma(\tau^- \to \nu_\tau + \text{hadrons})}{\Gamma(\tau^- \to \nu_\tau e^- \bar{\nu}_e)} \approx N_C = 3, \qquad (1.6)$$

which should be compared with the experimental averages [10]:

$$B_{\tau \to e} = (18.01 \pm 0.18)\%, \qquad B_{\tau \to \mu} = (17.65 \pm 0.24)\%, \qquad (1.7)$$

$$R_\tau = (1 - B_{\tau \to e} - B_{\tau \to \mu})/B_{\tau \to e} = 3.56 \pm 0.04. \qquad (1.8)$$

The agreement is fairly good. Taking $N_C = 3$, the naive predictions only deviate from the measured values by about 20%. Many other observables, such as the partial widths of the Z and $W^\pm$ bosons, can be analyzed in a similar way to conclude that $N_C = 3$.

A particularly strong test is obtained from the $\pi^0 \to \gamma\gamma$ decay, which occurs through the triangular quark loops in Fig. 5. The crossed vertex denotes the axial current $A_\mu^3 \equiv (\bar{u}\gamma_\mu\gamma_5 u - \bar{d}\gamma_\mu\gamma_5 d)$. One gets:

$$\Gamma(\pi^0 \to \gamma\gamma) = \left(\frac{N_C}{3}\right)^2 \frac{\alpha^2 m_\pi^3}{64\pi^3 f_\pi^2} = 7.73\, eV, \qquad (1.9)$$

where the π^0 coupling to A_μ^3, $f_\pi = 92.4$ MeV, is known from the $\pi^- \to \mu^- \bar{\nu}_\mu$ decay rate (assuming isospin symmetry). The agreement with the measured value, $\Gamma = 7.7 \pm 0.6$ eV [10], is remarkable. With $N_C = 1$, the prediction would have failed by a factor of 9. The nice thing about this decay is that it is associated with an *anomaly*: a global flavour
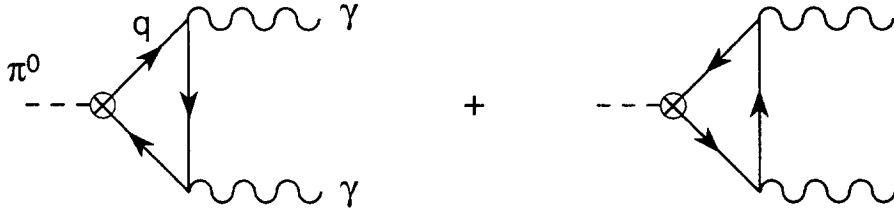
Figure 5: Triangular quark loops generating the decay $\pi^0 \to \gamma\gamma$.

symmetry which is broken by quantum effects (the triangular loops). One can then proof that the decay amplitude (1.9) does not get corrected by strong interactions [13].

Anomalies provide another compelling theoretical reason to adopt $N_C = 3$. The gauge symmetries of the Standard Model of electroweak interactions have also anomalies associated with triangular fermion loops (diagrams of the type shown in Fig. 5, but with arbitrary gauge bosons $-W^\pm, Z, \gamma-$ in the external legs and Standard Model fermions in the internal lines). These gauge anomalies are deathly because they destroy the renormalizability of the theory. Fortunately, the sum of all possible triangular loops cancels if $N_C = 3$. Thus, with three colours, anomalies are absent and the Standard Model is well-defined.

1.2 Asymptotic Freedom

The structure of the proton can be probed through the scattering $e^- p \to e^- p$. The cross-section is given by

$$\frac{d\sigma}{dQ^2} = \frac{\pi\alpha^2 \cos^2\frac{\theta}{2}}{4E^2 \sin^4\frac{\theta}{2} EE'} \left\{ \frac{|G_E(Q^2)|^2 + \frac{Q^2}{4M_p^2}|G_M(Q^2)|^2}{1 + \frac{Q^2}{4M_p^2}} + \frac{Q^2}{2M_p^2}|G_M(Q^2)|^2 \tan^2\frac{\theta}{2} \right\}, \quad (1.10)$$

where E and E' are the energies of the incident and scattered electrons, respectively, in the proton rest-frame, θ the scattering angle, M_p the proton mass and

$$Q^2 \equiv -q^2 = 4EE' \sin^2\frac{\theta}{2}, \quad (1.11)$$

with $q^\mu \equiv (k_e - k'_e)^\mu$ the momentum transfer through the intermediate photon propagator.

G_E and G_M are the electric and magnetic form factors, respectively, describing the proton electromagnetic structure; they would be equal to one for a pointlike spin-$\frac{1}{2}$ target. Experimentally they are known to be very well approximated by the dipole form

$$G_M(Q^2)/\mu_p \approx G_E(Q^2) \approx \left(1 + \frac{Q^2}{0.7\,\text{GeV}^2}\right)^{-2}, \quad (1.12)$$

where $\mu_p = 2.79$ is the proton magnetic moment (in proton Bohr magneton units). Thus, the proton is actually an extended object with a size of the order of 1 fm. At very low energies ($Q^2 \ll 1\,\text{GeV}^2$), the photon probe is unable to get information on the proton structure, $G_{M,E}(Q^2) \approx G_{M,E}(0) = 1$, and the proton behaves as a pointlike particle. At higher energies, the photon is sensitive to shorter distances; the proton finite size gives then rise to form factors, which suppress the elastic cross-section at large Q^2, i.e. at large angles.
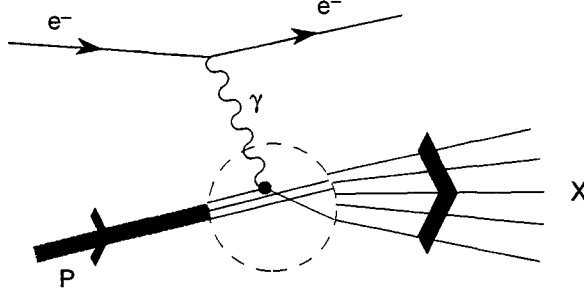
Figure 6: Inelastic $e^- p \to e^- X$ scattering.

One can try to further resolve the proton structure, by increasing the incident energy. The inelastic scattering $e^- p \to e^- X$ becomes then the dominant process. Making an inclusive sum over all hadrons produced, one has an additional kinematical variable corresponding to the final hadronic mass, $W^2 \equiv P_X^2$. The scattering is usually described in terms of Q^2 and

$$\nu \equiv \frac{(P \cdot q)}{M_p} = \frac{Q^2 + W^2 - M_p^2}{2M_p} = E - E' , \qquad (1.13)$$

where P^μ is the proton cuadrimomentum; ν is the energy transfer in the proton rest-frame. In the one-photon approximation, the unpolarized differential cross-section is given by

$$\frac{d\sigma}{dQ^2 \, d\nu} = \frac{\pi \alpha^2 \cos^2\frac{\theta}{2}}{4E^2 \sin^4\frac{\theta}{2} E E'} \left\{ W_2(Q^2,\nu) + 2\, W_1(Q^2,\nu) \tan^2\frac{\theta}{2} \right\} . \qquad (1.14)$$

The proton structure is then characterized by two measurable *structure functions*. For a pointlike proton, the elastic scattering (1.10) corresponds to

$$W_1(Q^2,\nu) = \frac{Q^2}{4M_p^2} \delta\left(\nu - \frac{Q^2}{2M_p}\right) , \qquad W_2(Q^2,\nu) = \delta\left(\nu - \frac{Q^2}{2M_p}\right) . \qquad (1.15)$$

At low Q^2, the experimental data reveals prominent resonances; but this resonance structure quickly dies out as Q^2 increases. A much softer but sizeable continuum contribution persists at large Q^2, suggesting the existence of pointlike objects inside the proton.

To get an idea of the possible behaviour of the structure functions, one can make a very rough model of the proton, assuming that it consist of some number of pointlike spin-$\frac{1}{2}$ constituents (the so-called *partons*), each one carrying a given fraction ξ_i of the proton momenta, i.e. $p_i{}^\mu = \xi_i P^\mu$. That means that we are neglecting[1] the transverse parton momenta, and $m_i = \xi M_p$. The interaction of the photon-probe with the parton i generates a contribution to the structure functions given by:

$$W_1^{(i)}(Q^2,\nu) = \frac{e_i^2 Q^2}{4m_i^2} \delta\left(\nu - \frac{Q^2}{2m_i}\right) = \frac{e_i^2}{2M_p} \delta\left(\xi_i - x\right), \qquad (1.16)$$

$$W_2^{(i)}(Q^2,\nu) = e_i^2 \delta\left(\nu - \frac{Q^2}{2m_i}\right) = e_i^2 \frac{x}{\nu} \delta\left(\xi_i - x\right), \qquad (1.17)$$

---

1) These approximations can be made more precise going to the infinite momentum frame of the proton, where the transverse motion is negligible compared with the large longitudinal boost of the partons.

where e_i is the parton electric charge and

$$x \equiv \frac{Q^2}{2M_p \nu} = \frac{Q^2}{Q^2 + W^2 - M_p^2} \,. \tag{1.18}$$

Thus, the parton structure functions only depend on the ratio x, which, moreover, fixes the momentum fractions ξ_i. We can go further, and assume that in the limit $Q^2 \to \infty$, $\nu \to \infty$, but keeping x fixed, the proton structure functions can be estimated from an incoherent sum of the parton ones (neglecting any strong interactions among the partons). Denoting $f_i(\xi_i)$ the probability that the parton i has momentum fraction ξ_i, one then has:

$$W_1(Q^2, \nu) = \sum_i \int_0^1 d\xi_i \, f_i(\xi_i) \, W_1^{(i)}(Q^2, \nu) = \frac{1}{2M_p} \sum_i e_i^2 f_i(x) \equiv \frac{1}{M_p} F_1(x)\,, \tag{1.19}$$

$$W_2(Q^2, \nu) = \sum_i \int_0^1 d\xi_i \, f_i(\xi_i) \, W_2^{(i)}(Q^2, \nu) = \frac{x}{\nu} \sum_i e_i^2 f_i(x) \equiv \frac{1}{\nu} F_2(x)\,. \tag{1.20}$$

This simple parton description implies then the so-called Bjorken *scaling* [14]: the proton structure functions only depend on the kinematical variable x. Moreover, one gets the Callan–Gross relation [15]

$$F_2(x) = 2x F_1(x)\,, \tag{1.21}$$

which is a consequence of our assumption of spin-$\frac{1}{2}$ partons. It is easy to check that spin-0 partons would have lead to $F_1(x) = 0$.
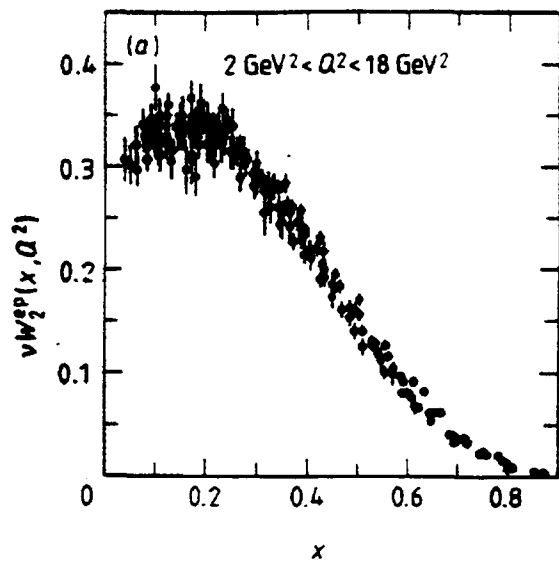

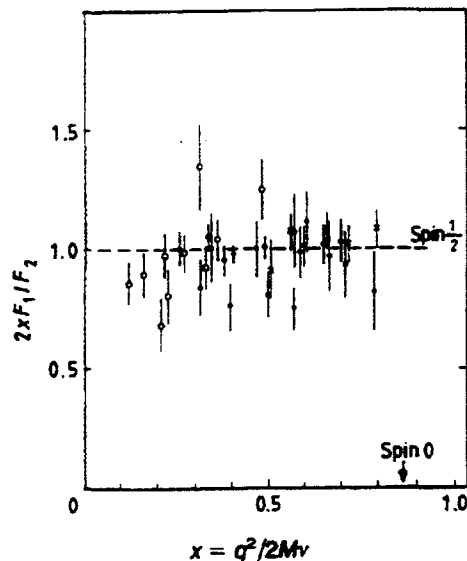Figure 7: Experimental data on νW_2 as function of x, for different values of Q^2 [16] (taken from Ref. [1]).

Figure 8: The ratio $2x F_1/F_2$ versus x, for different Q^2 values (1.5 GeV$^2 < Q^2 < 16$ GeV^2) [17] (taken from Ref. [1]).

The measured values of $\nu W_2(Q^2, \nu)$ are shown in Fig. 7 as function of x, for many different values of Q^2 between 2 and 18 GeV^2; the concentration of data points along a curve indicates that Bjorken scaling is correct, to a quite good approximation. Fig. 8 shows that the Callan–Gross relation is also reasonably well satisfied by the data, supporting the spin-$\frac{1}{2}$ assignment for the partons.

The surprising thing of this successful predictions is that we have assumed the existence of free independent pointlike partons inside the proton, in spite of the fact that quarks are suposed to be confined by very strong colour forces. Bjorken scaling suggests that the strong interactions must have the property of *asymptotic freedom*: they should become weaker at short distances, so that quarks behave as free particles for $Q^2 \rightarrow \infty$. This also agrees with the empirical observation in Fig. 3, that the free-quark description of the ratio $R_{e^+e^-}$ works better at higher energies.

Thus, the interaction between a $q\bar{q}$ pair looks like some kind of rubber band. If we try to separate the quark form the antiquark the force joining them increases. At some point, the energy on the elastic band is bigger than $2m_{q'}$, so that it becomes energetically favourable to create an additional $q'\bar{q}'$ pair; then the band breaks down into two mesonic systems, $q\bar{q}'$ and $q'\bar{q}$, each one with its corresponding half-band joining the quark pair. Increasing more and more the energy, we can only produce more and more mesons, but quarks remain always confined within colour-singlet bound states. Conversely, if one tries to approximate two quark constituents into a very short-distance region, the elastic band loses the energy and becomes very soft; quarks behave then as free particles.

1.3 Why $SU(3)$?

Flavour-changing transitions have a much weaker strength than processes mediated by the strong force. The quark-flavour quantum number is associated with the electroweak interactions, while strong forces appear to be flavour-conserving and flavour-independent. On the other side, the carriers of the electroweak interaction (γ, Z, $W^\pm$) do not couple to the quark colour. Thus, it seems natural to take colour as the charge associated with the strong forces and try to build a quantum field theory based on it [18]. The empirical evidence described so far puts a series of requirements that the fundamental theory of colour interactions should satisfy:

1. Colour is an exact symmetry G_C (hadrons do not show colour multiplicity).
2. $N_C = 3$. Thus, quarks belong to the triplet representation $\underline{3}$ of G_C.
3. Quarks and antiquarks are different states. Therefore, $\underline{3}^* \neq \underline{3}$, i.e. the triplet representation has to be complex.
4. Confinement hypothesis: hadronic states are colour singlets.
5. Asymptotic freedom.

Among all compact simple Lie groups there are only four having 3-dimensional irreducible representations; moreover, three of them are isomorphic to each other. Thus, we have only two choices: $SU(3)$ or $SO(3) \simeq SU(2) \simeq Sp(1)$. Since the triplet representation of $SO(3)$ is real, only the symmetry group $SU(3)$ survives the conditions 1, 2 and 3. The well-known $SU(3)$ decomposition of the products of $\underline{3}$ and $\underline{3}^*$ representations,

$$
\begin{aligned}
q\bar{q}: & \quad \underline{3} \otimes \underline{3}^* = \underline{1} \oplus \underline{8}\,, \\
qqq: & \quad \underline{3} \otimes \underline{3} \otimes \underline{3} = \underline{1} \oplus \underline{8} \oplus \underline{8} \oplus \underline{10}\,, \\
qq: & \quad \underline{3} \otimes \underline{3} = \underline{3}^* \oplus \underline{6}\,, \\
qqqq: & \quad \underline{3} \otimes \underline{3} \otimes \underline{3} \otimes \underline{3} = \underline{3} \oplus \underline{3} \oplus \underline{3} \oplus \underline{6}^* \oplus \underline{15} \oplus \underline{15} \oplus \underline{15} \oplus \underline{15}'\,,
\end{aligned}
\tag{1.22}
$$

guarantees that there are colour-singlet configurations corresponding to meson ($q\bar{q}$) and baryon (qqq) states, as required by the confinement hypothesis. Other exotic combinations such as diquarks (qq, $\bar{q}\bar{q}$) or four-quark states ($qqqq$, $\bar{q}\bar{q}\bar{q}\bar{q}$) do not satisfy this requirement.

Clearly, the theory of colour interactions should be based on the $SU(3)_C$ group. It remains to be seen whether such a theory is able to explain confinement and asymptotic freedom as natural dynamical consequences of the colour forces.

2. GAUGE SYMMETRY: QED

Let us consider the Lagrangian describing a free Dirac fermion:

$$\mathcal{L}_0 = i\,\overline{\Psi}(x)\gamma^\mu\partial_\mu\Psi(x) - m\,\overline{\Psi}(x)\Psi(x)\,. \tag{2.1}$$

$\mathcal{L}_0$ is invariant under *global* $U(1)$ transformations

$$\Psi(x) \xrightarrow{\mathrm{U}(1)} \Psi'(x) \equiv \exp\left\{iQ\theta\right\}\Psi(x)\,, \tag{2.2}$$

where $Q\theta$ is an arbitrary real constant. The phase of $\Psi(x)$ is then a pure convention-dependent quantity without physical meaning. However, the free Lagrangian is no-longer invariant if one allows the phase transformation to depend on the space-time coordinate, i.e. under *local* phase redefinitions $\theta = \theta(x)$, because

$$\partial_\mu\Psi(x) \xrightarrow{\mathrm{U}(1)} \exp\left\{iQ\theta\right\}\left(\partial_\mu + iQ\partial_\mu\theta\right)\Psi(x)\,. \tag{2.3}$$

Thus, once an observer situated at the point x_0 has adopted a given phase-convention, the same convention must be taken at all space-time points. This looks very unnatural.

The "Gauge Principle" is the requirement that the $U(1)$ phase invariance should hold *locally*. This is only possible if one adds some additional piece to the Lagrangian, transforming in such a way as to cancel the $\partial_\mu\theta$ term in Eq. (2.3). The needed modification is completely fixed by the transformation (2.3): one introduces a new spin–1 (since $\partial_\mu\theta$ has a Lorentz index) field $A_\mu(x)$, transforming as

$$A_\mu(x) \xrightarrow{\mathrm{U}(1)} A'_\mu(x) \equiv A_\mu(x) + \frac{1}{e}\partial_\mu\theta\,, \tag{2.4}$$

and defines the covariant derivative

$$D_\mu\Psi(x) \equiv \left[\partial_\mu - ieQA_\mu(x)\right]\Psi(x)\,, \tag{2.5}$$

which has the required property of transforming like the field itself:

$$D_\mu\Psi(x) \xrightarrow{\mathrm{U}(1)} \left(D_\mu\Psi\right)'(x) \equiv \exp\left\{iQ\theta\right\}D_\mu\Psi(x)\,. \tag{2.6}$$

The Lagrangian

$$\mathcal{L} \equiv i\,\overline{\Psi}(x)\gamma^\mu D_\mu\Psi(x) - m\,\overline{\Psi}(x)\Psi(x) = \mathcal{L}_0 + eQA_\mu(x)\,\overline{\Psi}(x)\gamma^\mu\Psi(x) \tag{2.7}$$

is then invariant under local $U(1)$ transformations.

The gauge principle has generated an interaction between the Dirac spinor and the gauge field A_μ, which is nothing else than the familiar QED vertex. Note that the corresponding electromagnetic charge eQ is completely arbitrary. If one wants A_μ to be a true propagating field, one needs to add a gauge-invariant kinetic term

$$\mathcal{L}_{\mathrm{Kin}} \equiv -\frac{1}{4}F_{\mu\nu}F^{\mu\nu}\,, \tag{2.8}$$

where $F_{\mu\nu} \equiv \partial_\mu A_\nu - \partial_\nu A_\mu$ is the usual electromagnetic field strength. A possible mass term for the gauge field, $\frac{1}{2}m^2 A^\mu A_\mu$, is forbidden because it would violate gauge invariance; therefore, the photon field is predicted to be massless. The total Lagrangian in (2.7) and (2.8) gives rise to the well-known Maxwell equations.

From a simple gauge-symmetry requirement, we have deduced the right QED Lagrangian, which leads to a very successful quantum field theory. Remember that QED predictions have been tested to a very high accuracy, as exemplified by the electron and muon anomalous magnetic moments $[a_l \equiv (g_l - 2)/2$, where $\mu_l \equiv g_l\,(e\hbar/2m_l)]$ [19]:

$$
a_e = \begin{cases} (115\,965\,214.0 \pm 2.8) \times 10^{-11} & \text{(Theory)} \\ (115\,965\,219.3 \pm 1.0) \times 10^{-11} & \text{(Experiment)} \end{cases}, \tag{2.9}
$$

$$
a_\mu = \begin{cases} (1\,165\,919.2 \pm 1.9) \times 10^{-9} & \text{(Theory)} \\ (1\,165\,923.0 \pm 8.4) \times 10^{-9} & \text{(Experiment)} \end{cases}. \tag{2.10}
$$

3. THE QCD LAGRANGIAN

Let us denote q_f^α a quark field of colour α and flavour f. To simplify the equations, let us adopt a vector notation in colour space: $q_f \equiv \mathrm{column}(q_f^1, q_f^2, q_f^3)$. The free Lagrangian

$$
\mathcal{L}_0 = \sum_f \bar{q}_f \left(i\gamma^\mu \partial_\mu - m_f \right) q_f \tag{3.1}
$$

is invariant under arbitrary global $SU(3)_C$ transformations in colour space,

$$
q_f^\alpha \longrightarrow (q_f^\alpha)' = U^\alpha{}_\beta\, q_f^\beta, \qquad UU^\dagger = U^\dagger U = 1, \qquad \det U = 1. \tag{3.2}
$$

The $SU(3)_C$ matrices can be written in the form

$$
U = \exp\left\{ -ig_s \frac{\lambda^a}{2}\theta_a \right\}, \tag{3.3}
$$

where λ^a ($a = 1, 2, \ldots, 8$) denote the generators of the fundamental representation of the $SU(3)_C$ algebra, and θ_a are arbitrary parameters. The matrices λ^a are traceless and satisfy the commutation relations

$$
\left[\lambda^a, \lambda^b \right] = 2i f^{abc} \lambda^c, \tag{3.4}
$$

with f^{abc} the $SU(3)_C$ structure constants, which are real and totally antisymmetric. Some useful properties of $SU(3)$ matrices are collected in Appendix A.

As in the QED case, we can now require the Lagrangian to be also invariant under local $SU(3)_C$ transformations, $\theta_a = \theta_a(x)$. To satisfy this requirement, we need to change the quark derivatives by covariant objects. Since we have now 8 independent gauge parameters, 8 different gauge bosons $G_a^\mu(x)$, the so-called *gluons*, are needed:

$$
D^\mu q_f \equiv \left[\partial^\mu - ig_s \frac{\lambda^a}{2} G_a^\mu(x) \right] q_f \equiv \left[\partial^\mu - ig_s G^\mu(x) \right] q_f. \tag{3.5}
$$

Notice that we have introduced the compact matrix notation

$$
[G^\mu(x)]_{\alpha\beta} \equiv \left(\frac{\lambda^a}{2} \right)_{\alpha\beta} G_a^\mu(x). \tag{3.6}
$$

We want $D^\mu q_f$ to transform in exactly the same way as the colour-vector q_f; this fixes the transformation properties of the gauge fields:

$$D^\mu \longrightarrow (D^\mu)' = U\,D^\mu\,U^\dagger\,; \qquad G^\mu \longrightarrow (G^\mu)' = U\,G^\mu\,U^\dagger - \frac{i}{g_s}\,(\partial^\mu U)\,U^\dagger\,. \tag{3.7}$$

Under an infinitesimal $SU(3)_C$ transformation,

$$q_f^\alpha \longrightarrow (q_f^\alpha)' = q_f^\alpha - ig_s \left(\frac{\lambda^a}{2}\right)_{\alpha\beta} \delta\theta_a\, q_f^\beta\,,$$

$$G_a^\mu \longrightarrow (G_a^\mu)' = G_a^\mu - \partial^\mu(\delta\theta_a) + g_s f^{abc}\delta\theta_b\, G_c^\mu\,. \tag{3.8}$$

The gauge transformation of the gluon fields is more complicated that the one obtained in QED for the photon. The non-commutativity of the $SU(3)_C$ matrices gives rise to an additional term involving the gluon fields themselves. For constant $\delta\theta_a$, the transformation rule for the gauge fields is expressed in terms of the structure constants f^{abc} only; thus, the gluon fields belong to the adjoint representation of the colour group (see Appendix A). Note also that there is a unique $SU(3)_C$ coupling g_s. In QED it was possible to assign arbitrary electromagnetic charges to the different fermions. Since the commutation relation (3.4) is non-linear, this freedom does not exist for $SU(3)_C$.

To build a gauge-invariant kinetic term for the gluon fields, we introduce the corresponding field strengths:

$$G^{\mu\nu}(x) \equiv \frac{i}{g_s}[D^\mu, D^\nu] = \partial^\mu G^\nu - \partial^\nu G^\mu - ig_s\,[G^\mu, G^\nu] \equiv \frac{\lambda^a}{2}\,G_a^{\mu\nu}(x)\,,$$

$$G_a^{\mu\nu}(x) = \partial^\mu G_a^\nu - \partial^\nu G_a^\mu + g_s f^{abc} G_b^\mu G_c^\nu\,. \tag{3.9}$$

Under a gauge transformation,

$$G^{\mu\nu} \longrightarrow (G^{\mu\nu})' = U\,G^{\mu\nu}\,U^\dagger\,, \tag{3.10}$$

and the colour trace $\text{Tr}(G^{\mu\nu}G_{\mu\nu}) = \frac{1}{2}G_a^{\mu\nu}G_{\mu\nu}^a$ remains invariant.

Taking the proper normalization for the gluon kinetic term, we finally have the $SU(3)_C$ invariant QCD Lagrangian:

$$\mathcal{L}_{\text{QCD}} \equiv -\frac{1}{4}\,G_a^{\mu\nu}G_{\mu\nu}^a + \sum_f \bar{q}_f\,(i\gamma^\mu D_\mu - m_f)\,q_f\,. \tag{3.11}$$

It is worth while to decompose the Lagrangian into its different pieces:

$$\mathcal{L}_{\text{QCD}} = -\frac{1}{4}(\partial^\mu G_a^\nu - \partial^\nu G_a^\mu)(\partial_\mu G_\nu^a - \partial_\nu G_\mu^a) + \sum_f \bar{q}_f^\alpha\,(i\gamma^\mu \partial_\mu - m_f)\,q_f^\alpha$$

$$+ g_s\, G_a^\mu \sum_f \bar{q}_f^\alpha \gamma_\mu \left(\frac{\lambda^a}{2}\right)_{\alpha\beta} q_f^\beta \tag{3.12}$$

$$- \frac{g_s}{2}\, f^{abc}\,(\partial^\mu G_a^\nu - \partial^\nu G_a^\mu)\, G_\mu^b G_\nu^c - \frac{g_s^2}{4}\, f^{abc} f_{ade}\, G_b^\mu G_c^\nu G_\mu^d G_\nu^e\,.$$

The first line contains the correct kinetic terms for the different fields, which give rise to the corresponding propagators. The colour interaction between quarks and gluons is given

by the second line; it involves the $SU(3)_C$ matrices λ^a. Finally, owing to the non-abelian character of the colour group, the $G_a^{\mu\nu}G_{\mu\nu}^a$ term generates the cubic and quartic gluon self-interactions shown in the last line; the strength of these interactions is given by the same coupling g_s which appears in the fermionic piece of the Lagrangian.

In spite of the rich physics contained in it, the Lagrangian (3.11) looks very simple, because of its colour-symmetry properties. All interactions are given in terms of a single universal coupling g_s, which is called the *strong coupling constant*. The existence of self-interactions among the gauge fields is a new feature that was not present in the QED case; it seems then reasonable to expect that these gauge self-interactions could explain properties like asymptotic freedom and confinement, which do not appear in QED.
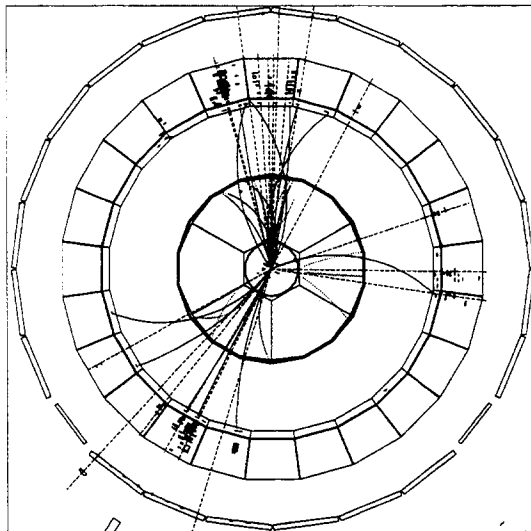

Figure 9: Three-jet event from the hadronic decay of a Z boson (DELPHI).

Without any detailed calculation, one can already extract qualitative physical consequences from $\mathcal{L}_{\text{QCD}}$. Quarks can emit gluons. At lowest-order in g_s, the dominant process will be the emission of a single gauge boson. Thus, the hadronic decay of the Z should result in some $Z \to q\bar{q}G$ events, in addition to the dominant $Z \to q\bar{q}$ decays discussed in Section 1. Fig. 9 clearly shows that 3-jet events, with the required kinematics, indeed appear in the LEP data. Similar events show up in e^+e^- annihilation into hadrons, away from the Z peak.

In order to properly quantize the QCD Lagrangian, one needs to add to $\mathcal{L}_{\text{QCD}}$ the so-called *Gauge-fixing* and *Faddeev–Popov* terms. Since this is a rather technical issue, its discussion is relegated to Appendix B.

4.   QUANTUM LOOPS

The QCD Lagrangian is rather economic in the sense that it involves a single coupling g_s. Thus, all strong-interacting phenomena should be described in terms of just one parameter. At lowest order in g_s (tree-level), it is straightforward to compute all kind of scattering amplitudes involving quarks and gluons: $q\bar{q} \to GG$, $qq \to qq$, $Gq \to Gq$, ... Unfortunately, this exercise by itself does not help very much to understand the physical hadronic world. First, we see hadrons instead of quarks and gluons. Second, we have learnt from experiment that the strength of the strong forces changes with the

168

energy scale: the interaction is very strong (confining) at low energies, but quarks behave as nearly free particles at high energies. Obviously, we cannot understand both energy regimes with a single constant g_s, which is the same everywhere. Moreover, if we neglect the quark masses, the QCD Lagrangian does not contain any energy scale; thus, there is no way to decide when the energy of a given process is large or small, because we do not have any reference scale to compare with.

If QCD is the right theory of the strong interactions, it should provide some dynamical scale through quantum effects.

4.1 Regularization of loop integrals

The computation of perturbative corrections to the tree-level results involves divergent loop integrals. It is then necessary to find a way of getting finite results with physical meaning from a priori meaningless divergent quantities.
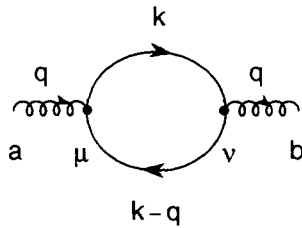

Figure 10: Gluon self-energy diagram.

Let us consider the self-energy gluon loop in Fig. 10. The corresponding contribution in momentum space can be easily obtained, using standard Feynman rules techniques:

$$i\Pi_{ab}^{\mu\nu}(q) = -g_s^2 \delta_{ab} T_F \int \frac{d^4k}{(2\pi)^4} \frac{\mathrm{Tr}[\gamma^\mu \slashed{k} \gamma^\nu (\slashed{k} - \slashed{q})]}{k^2 (k-q)^2}. \tag{4.1}$$

The result is proportional to g_s^2, because there are two $q\bar{q}G$ vertices, and there is a trivial $SU(3)_C$ factor, $T_F = \frac{1}{2}$, coming from the colour trace $\frac{1}{4}\mathrm{Tr}(\lambda^a \lambda^b) = \delta^{ab} T_F$.

The problem appears in the momentum integration, which is clearly divergent $[\sim \int d^4k(1/k^2) = \infty]$. We can define the momentum integral in many different (and arbitrary) ways. For instance, we could introduce a *cut-off M*, such that only momentum scales smaller than M are integrated; obviously, the resulting integral would be an increasing function of M. Instead, it has become conventional to define the loop integrals through *dimensional regularization*: the calculation is performed in $D = 4 + 2\epsilon$ dimensions. For $\epsilon \neq 0$ the resulting integral is well-defined:

$$\int \frac{d^D k}{(2\pi)^D} \frac{k^\alpha (k-q)^\beta}{k^2 (k-q)^2} = \frac{-i}{6(4\pi)^2} \left(\frac{-q^2}{4\pi} \right)^\epsilon \Gamma(-\epsilon) \left(1 - \frac{5}{3}\epsilon \right) \left\{ \frac{q^2 g^{\alpha\beta}}{2(1+\epsilon)} + q^\alpha q^\beta \right\}. \tag{4.2}$$

The ultraviolet divergence of the loop appears at $\epsilon = 0$, through the pole of the Gamma function,

$$\Gamma(-\epsilon) = -\frac{1}{\epsilon} - \gamma_E + \mathcal{O}(\epsilon^2), \tag{4.3}$$

where $\gamma_E = 0.577215\ldots$ is the Euler constant.

Although the integral (4.2) looks somewhat funny, dimensional regularization has many advantages because does not spoil the gauge symmetry of QCD and, therefore, simplifies a lot the calculations. One could argue that a cut-off procedure would be more *physical*, since the parameter M could be related to some unknown additional physics at very short distances. However, within the QCD framework, both prescriptions are equally meaningless. One just introduces a regularizing parameter, such that the integral is well-defined and the divergence is recovered in some limit ($M \to \infty$ or $\epsilon \to 0$).

Since the momentum-transfer q^2 has dimensions, it turns out to be convenient to introduce and arbitrary energy scale μ and write

$$\left(\frac{-q^2}{4\pi}\right)^\epsilon \Gamma(-\epsilon) = \mu^{2\epsilon}\left(\frac{-q^2}{4\pi\mu^2}\right)^\epsilon \Gamma(-\epsilon) = -\mu^{2\epsilon}\left\{\frac{1}{\epsilon} + \gamma_E - \ln 4\pi + \ln\left(-q^2/\mu^2\right) + \mathcal{O}(\epsilon)\right\}. \tag{4.4}$$

Obviously, this expression does not depend on μ; but written in this form one has a dimensionless quantity $(-q^2/\mu^2)$ inside the logarithm.

The contribution of the loop diagram in Fig. 10 can finally be written as

$$\Pi_{ab}^{\mu\nu} = \delta_{ab}\left(-q^2 g^{\mu\nu} + q^\mu q^\nu\right)\Pi(q^2),$$

$$\Pi(q^2) = -\frac{4}{3}T_F\left(\frac{g_s\mu^\epsilon}{4\pi}\right)^2\left\{\frac{1}{\epsilon} + \gamma_E - \ln 4\pi + \ln\left(-q^2/\mu^2\right) - \frac{5}{3} + \mathcal{O}(\epsilon)\right\}. \tag{4.5}$$

Owing to the ultraviolet divergence, Eq. (4.5) does not determine the wanted self-energy contribution. Nevertheless, it does show how this effect changes with the energy scale. If one could fix the value of $\Pi(q^2)$ at some reference momentum transfer q_0^2, the result would be known at any other scale:

$$\Pi(q^2) = \Pi(q_0^2) - \frac{4}{3}T_F\left(\frac{g_s}{4\pi}\right)^2\ln\left(q^2/q_0^2\right). \tag{4.6}$$

We can split the self-energy contribution into a meaningless divergent piece and a finite term, which includes the q^2 dependence,

$$\Pi(q^2) \equiv \Delta\Pi_\epsilon(\mu^2) + \Pi_R(q^2/\mu^2). \tag{4.7}$$

This separation is of course ambiguous, because the finite q^2-independent contributions can be splitted in many different ways. A given choice defines a *scheme*:

$$\Delta\Pi_\epsilon(\mu^2) = \begin{cases} -\frac{T_F}{3\pi}\frac{g_s^2}{4\pi}\mu^{2\epsilon}\left[\frac{1}{\epsilon} + \gamma_E - \ln(4\pi) - \frac{5}{3}\right] & (\mu\text{-scheme}), \\ -\frac{T_F}{3\pi}\frac{g_s^2}{4\pi}\mu^{2\epsilon}\frac{1}{\epsilon} & (\text{MS-scheme}), \\ -\frac{T_F}{3\pi}\frac{g_s^2}{4\pi}\mu^{2\epsilon}\left[\frac{1}{\epsilon} + \gamma_E - \ln(4\pi)\right] & (\overline{\text{MS}}\text{-scheme}), \end{cases} \tag{4.8}$$

$$\Pi_R(q^2/\mu^2) = \begin{cases} -\frac{T_F}{3\pi}\frac{g_s^2}{4\pi}\ln\left(-q^2/\mu^2\right) & (\mu\text{-scheme}), \\ -\frac{T_F}{3\pi}\frac{g_s^2}{4\pi}\left[\ln\left(-q^2/\mu^2\right) + \gamma_E - \ln(4\pi) - \frac{5}{3}\right] & (\text{MS-scheme}), \\ -\frac{T_F}{3\pi}\frac{g_s^2}{4\pi}\left[\ln\left(-q^2/\mu^2\right) - \frac{5}{3}\right] & (\overline{\text{MS}}\text{-scheme}). \end{cases} \tag{4.9}$$

In the μ-scheme, one uses the value of $\Pi(-\mu^2)$ to define the divergent part. MS and $\overline{\text{MS}}$ stand for minimal subtraction [20] and modified minimal subtraction schemes [21]; in the MS case, one subtracts only the divergent $1/\epsilon$ term, while the $\overline{\text{MS}}$ scheme puts also the annoying $\gamma_E - \ln(4\pi)$ factor into the divergent part. Notice that the logarithmic q^2-dependence is always the same.
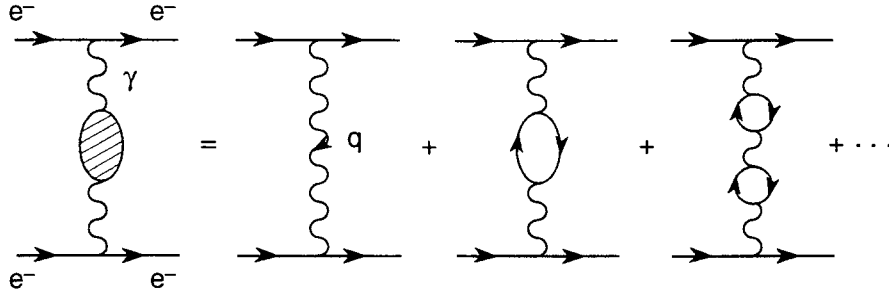
Figure 11: Photon self-energy contribution to $e^- e^-$ scattering.

4.2 Renormalization: QED

A Quantum Field Theory is called *renormalizable* if all ultraviolet divergences can be reabsorbed through a redefinition of the original fields and couplings.

Let us consider the electromagnetic interaction between two electrons. At one loop, the QED photon self-energy contribution is just given by Eq. 4.5, with the changes $T_F \to 1$ and $g_s \to e$. The corresponding scattering amplitude takes the form

$$T(q^2) \sim -J^\mu J_\mu \frac{e^2}{q^2} \left\{ 1 - \Pi(q^2) + \ldots \right\} ,$$ (4.10)

where J^μ denotes the electromagnetic fermion current.

At lowest order, $T(q^2) \sim \alpha/q^2$ with $\alpha = e^2/(4\pi)$. The divergent correction generated by quantum loops can be reabsorbed into a redefinition of the coupling:

$$\frac{\alpha_0}{q^2} \left\{ 1 - \Delta\Pi_\epsilon(\mu^2) - \Pi_R(q^2/\mu^2) \right\} \equiv \frac{\alpha_R(\mu^2)}{q^2} \left\{ 1 - \Pi_R(q^2/\mu^2) \right\} ,$$ (4.11)

$$\alpha_R(\mu^2) = \alpha_0 \left\{ 1 + \frac{\alpha_0}{3\pi} \mu^{2\epsilon} \left[\frac{1}{\epsilon} + C_{\text{scheme}} \right] + \ldots \right\} , \qquad \alpha_0 \equiv \frac{e_0^2}{4\pi} ,$$ (4.12)

where e_0 denotes the *bare* coupling appearing in the QED Lagrangian; this bare quantity is, however, not directly observable. Making the redefinition (4.11), the scattering amplitude is finite and gives rise to a definite prediction for the cross-section, which can be compared with experiment; thus, one actually measures the *renormalized* coupling α_R.

The redefinition (4.11) is meaningful, provided that it can be done in a self-consistent way: all ultraviolet divergent contributions to all possible scattering processes should be eliminated through the same redefinition of the coupling (and the fields). The nice thing of gauge theories, such as QED or QCD, is that the underlying gauge symmetry guarantees the renormalizability of the quantum field theory.

The renormalized coupling $\alpha_R(\mu^2)$ depends on the arbitrary scale μ and on the chosen *renormalization scheme* [the constant C_{scheme} denotes the different finite terms in Eq. (4.8)]. Quantum loops have introduced a scale dependence in a quite subtle way. Both $\alpha_R(\mu^2)$ and the renormalized self-energy correction $\Pi_R(q^2/\mu^2)$ depend on μ, but the physical scattering amplitude $T(q^2)$ is of course μ-independent: $(Q^2 \equiv -q^2)$

$$\begin{aligned} T(q^2) &\sim -4\pi J^\mu J_\mu \frac{\alpha_R(\mu^2)}{q^2} \left\{ 1 + \frac{\alpha_R(\mu^2)}{3\pi} \left[\ln\left(\frac{-q^2}{\mu^2} \right) + C'_{\text{scheme}} \right] + \ldots \right\} \\ &= 4\pi J^\mu J_\mu \frac{\alpha_R(Q^2)}{Q^2} \left\{ 1 + \frac{\alpha_R(Q^2)}{3\pi} C'_{\text{scheme}} + \cdots \right\} . \end{aligned}$$ (4.13)

171

The quantity $\alpha(Q^2) \equiv \alpha_R(Q^2)$ is called the QED *running coupling*. The ordinary fine structure constant $\alpha = 1/137$ is defined through the classical Thomson formula; therefore, it corresponds to a very low scale $Q^2 = -m_e^2$. Clearly, the value of α relevant for LEP experiments is not the same $[\alpha(M_Z^2)_{\overline{\text{MS}}} = 1/129]$. The scale dependence of $\alpha(Q^2)$ is regulated by the so-called β-function:

$$\mu \frac{d\alpha}{d\mu} \equiv \alpha\beta(\alpha); \qquad \beta(\alpha) = \beta_1 \frac{\alpha}{\pi} + \beta_2 \left(\frac{\alpha}{\pi}\right)^2 + \cdots \qquad (4.14)$$

At the one-loop level, the β-function reduces to the first coefficient, which is fixed by Eq. (4.12):

$$\beta_1^{\text{QED}} = \frac{2}{3}. \qquad (4.15)$$

The first-order differential equation (4.14) can then be easily solved, with the result:

$$\alpha(Q^2) = \frac{\alpha(Q_0^2)}{1 - \frac{\beta_1\alpha(Q_0^2)}{2\pi}\ln\left(Q^2/Q_0^2\right)}. \qquad (4.16)$$

Since $\beta_1 > 0$, the QED running coupling increases with the energy scale: $\alpha(Q^2) > \alpha(Q_0^2)$ if $Q^2 > Q_0^2$; i.e. the electromagnetic charge decreases at large distances. This can be intuitively understood as the screening effect due to the virtual e^+e^- pairs generated, through quantum effects, around the electron charge. The physical QED vacuum behaves as a polarized dielectric medium.
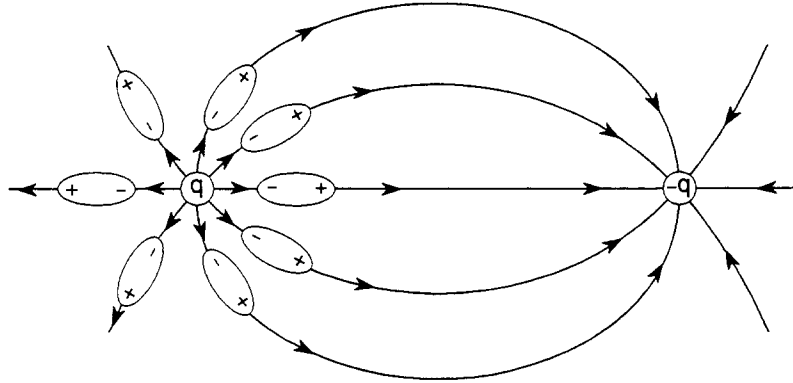

Figure 12: Electromagnetic charge screening in a dipolar medium.

Notice that taking $\mu^2 = Q^2$ in Eq. (4.13) we have eliminated all dependences on $\ln\left(Q^2/\mu^2\right)$ to all orders in α. The running coupling (4.16) makes a resummation of all leading logarithmic corrections, i.e

$$\alpha(Q^2) = \alpha(\mu^2) \sum_{n=0}^{\infty} \left[\frac{\beta_1\alpha(\mu^2)}{2\pi}\ln\left(Q^2/\mu^2\right)\right]^n. \qquad (4.17)$$

This higher-order logarithms correspond to the contributions from an arbitrary number of one-loop self-energy insertions along the intermediate photon propagator in Fig. 11 $[1 - \Pi_R(q^2/\mu^2) + (\Pi_R(q^2/\mu^2))^2 + \cdots]$.
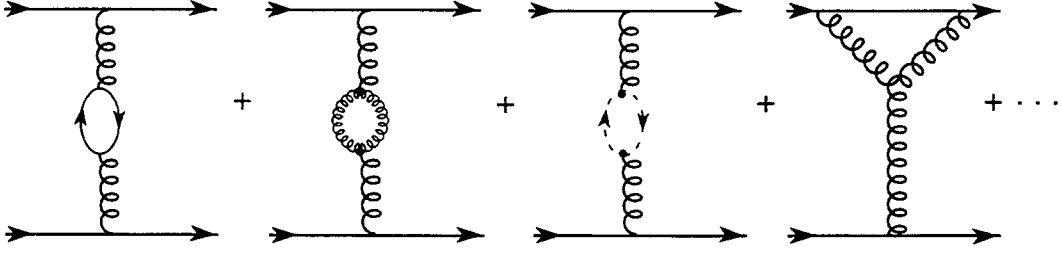
Figure 13: Feynman diagrams contributing to the renormalization of the strong coupling. The dashed loop indicates the *ghost* correction discussed in Appendix B.

4.3 The QCD running coupling

The renormalization of the QCD coupling proceeds in a similar way. Owing to the non-abelian character of $SU(3)_C$, there are additional contributions involving gluon self-interactions. From the calculation of the relevant one-loop diagrams, shown in Fig. 13, one gets the value of the first β-function coefficient [22,23]:

$$\beta_1 = \frac{2}{3}T_F N_f - \frac{11}{6}C_A = \frac{2N_f - 11N_C}{6}. \tag{4.18}$$

The positive contribution proportional to N_f is generated by the q-$\bar{q}$ loops and corresponds to the QED result (except for the T_F factor). The gluonic self-interactions introduce the additional *negative* contribution proportional to N_C. This second term is responsible for the completely different behaviour of QCD: $\beta_1 < 0$ if $N_f \leq 16$. The corresponding QCD running coupling,

$$\alpha_s(Q^2) = \frac{\alpha_s(Q_0^2)}{1 - \frac{\beta_1 \alpha_s(Q_0^2)}{2\pi} \ln\left(Q^2/Q_0^2\right)}, \tag{4.19}$$

decreases at short distances, i.e.

$$\lim_{Q^2 \to \infty} \alpha_s(Q^2) = 0. \tag{4.20}$$

Thus, for $N_f \leq 16$, QCD has indeed the required property of asymptotic freedom. The gauge self-interactions of the gluons *spread out* the QCD charge, generating an *antiscreening* effect. This could not happen in QED, because photons do not carry electric charge. Only non-abelian gauge theories, where the intermediate gauge bosons are self-interacting particles, have this antiscreening property [24].

Although quantum effects have introduced a dependence with the energy, we still need a reference scale to decide when a given Q^2 can be considered large or small. An obvious possibility is to choose the scale at which α_s enters into a strong-coupling regime (i.e. $\alpha_s \sim 1$), where perturbation theory is no longer valid. A more precise definition can be obtained from the solution of the β-function differential equation (4.14). At one loop, one gets

$$\ln \mu + \frac{\pi}{\beta_1 \alpha_s(\mu^2)} = \ln \Lambda, \tag{4.21}$$

where $\ln \Lambda$ is just an integration constant. Thus,

$$\alpha_s(\mu^2) = \frac{2\pi}{-\beta_1 \ln\left(\mu^2/\Lambda^2\right)}. \tag{4.22}$$

In this way, we have traded the dimensionless parameter g_s by the dimensionful scale Λ. The number of QCD free parameters is the same (1 for massless quarks), but quantum effects have generated an energy scale. Although, Eq. (4.19) gives the impression that the scale-dependence of $\alpha_s(\mu^2)$ involves two parameters, μ_0^2 and $\alpha_s(\mu_0^2)$, only the combination (4.21) is actually relevant, as explicitly shown in (4.22).

When $\mu \gg \Lambda$, $\alpha_s(\mu^2) \to 0$, so that we recover asymptotic freedom. At lower energies the running coupling gets bigger; for $\mu \to \Lambda$, $\alpha_s(\mu^2) \to \infty$ and perturbation theory breaks down. The scale Λ indicates when the strong coupling blows up. Eq. (4.22) suggests that confinement at low energies is quite plausible in QCD; however, it does not provide a proof because perturbation theory is no longer valid when $\mu \to \Lambda$.

4.4   Higher orders

Higher orders in perturbation theory are much more important in QCD than in QED, because the coupling is much bigger (at ordinary energies). Unfortunately, the calculations are also technically more involved. Nevertheless, many quantities have been already computed at $\mathcal{O}(\alpha_s^2)$ or even $\mathcal{O}(\alpha_s^3)$. The β-function is known to three loops; in the $\overline{\text{MS}}$ scheme, the computed higher-order coefficients take the values [25]:

$$\beta_2 = -\frac{51}{4} + \frac{19}{12} N_f; \qquad \beta_3 = \frac{1}{64}\left[-2857 + \frac{5033}{9} N_f - \frac{325}{27} N_f^2\right]. \qquad (4.23)$$

If $N_f \leq 8$, $\beta_2 < 0$ ($\beta_3 < 0$ for $N_f \leq 5$) which further reinforces the asymptotic freedom behaviour.

The scale dependence of the running coupling at higher-orders is given by:

$$\alpha_s(\mu^2) = \alpha_s(\mu_0^2)\left\{1 - \frac{\beta_1}{2}\frac{\alpha_s(\mu_0^2)}{\pi}\ln\left(\mu^2/\mu_0^2\right) - \frac{\beta_2}{2}\left(\frac{\alpha_s(\mu_0^2)}{\pi}\right)^2\ln\left(\mu^2/\mu_0^2\right) + \cdots\right\}^{-1}, \qquad (4.24)$$

or, in terms of Λ,

$$\alpha_s(\mu^2) = \frac{2\pi}{(-\beta_1)\ln\left(\mu^2/\Lambda^2\right)}\left\{1 - \frac{\beta_2}{\beta_1}\frac{2}{(-\beta_1)\ln\left(\mu^2/\Lambda^2\right)}\ln\left[\frac{1}{2}\ln\left(\mu^2/\Lambda^2\right)\right] + \cdots\right\}. \qquad (4.25)$$

When comparing different QCD fits to the data, it is worth while to have in mind that any given value of α_s refers to a particular selection of scale and renormalization scheme. Moreover, the resulting numerical values can be different if one works at leading (LO), next-to-leading (NLO) or next-to-next-to-leading (NNLO) order. Although the parameter Λ does not depend on the scale, it is a scheme-dependent quantity. For instance:

$$\Lambda_{\text{MS}}^2 = \frac{e^{\gamma_E}}{4\pi}\Lambda_{\overline{\text{MS}}}^2. \qquad (4.26)$$

Moreover, $\Lambda_{\text{LO}} \neq \Lambda_{\text{NLO}} \neq \Lambda_{\text{NNLO}}$. In fact, slightly different definitions of Λ can be given at NLO, depending on the way the integration constant is chosen when solving the β-function differential equation. Moreover, since in the MS and $\overline{\text{MS}}$ schemes the β-function coefficients depend on N_f, Λ takes different values when the number of flavours is changed. At NLO, the relation between the Λ scales for 3 and 4 flavours is given by:

$$\Lambda_4 \approx \Lambda_3\left(\frac{\Lambda_3}{m_c}\right)^{2/25}\left[\ln\left(m_c^2/\Lambda_3^2\right)\right]^{-107/1875}. \qquad (4.27)$$
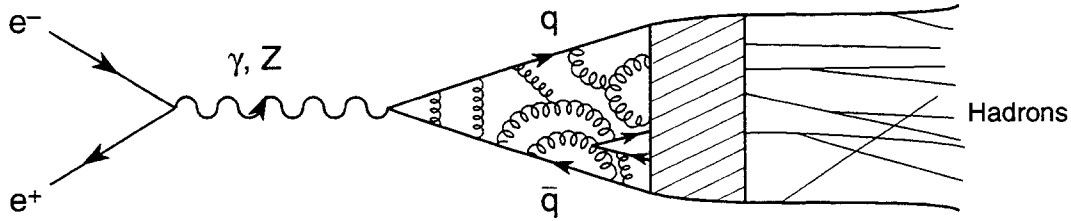
Figure 14: $e^+e^- \to \gamma^*, Z^* \to$ hadrons.

5. PERTURBATIVE QCD PHENOMENOLOGY

5.1 $e^+e^- \to$ hadrons

The inclusive production of hadrons in e^+e^- annihilation is a good process for testing perturbative QCD predictions. The hadronic production occurs through the basic mechanism $e^+e^- \to \gamma^*, Z^* \to q\bar{q}$, where the final q-$\bar{q}$ pair interacts through the QCD forces; thus, the quarks exchange and emit gluons (and q'-$\bar{q}'$ pairs) in all possible ways.

At high energies, where α_s is small, we can use perturbative techniques to predict the different subprocesses: $e^+e^- \to q\bar{q}, q\bar{q}G, q\bar{q}GG, \ldots$ However, we still do not have a good understanding of the way quarks and gluons hadronize. Qualitatively, quarks and gluons are created by the q-$\bar{q}$ current at very short distances, $x \sim 1/\sqrt{s}$. Afterwards, they continue radiating additional soft gluons with smaller energies. At larger distances, $x \sim 1/\Lambda$, the interaction becomes very strong and the hadronization process occurs. Since we are lacking a rigorous description of the confinement mechanism, we are unable to provide precise predictions of the different exclusive processes, such as $e^+e^- \to 16\pi$. However, we can make a quite accurate prediction for the total inclusive production of hadrons:

$$\sigma(e^+e^- \to \text{hadrons}) = \sigma(e^+e^- \to q\bar{q} + q\bar{q}G + q\bar{q}GG + \ldots). \tag{5.1}$$

The details of the final hadronization are irrelevant for the inclusive sum, because the probability to hadronize is just one owing to our confinement assumption.
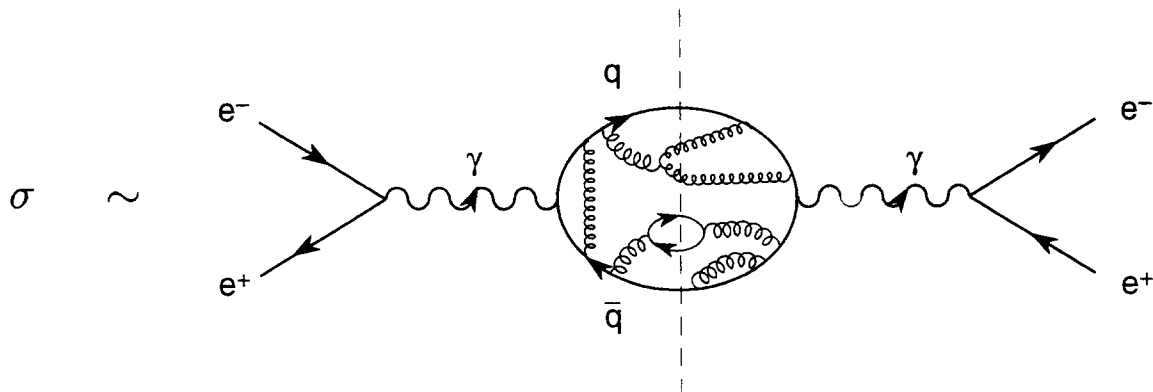

Figure 15: Diagrammatic relation between the total hadronic-production cross-section and the two-point function $\Pi^{\mu\nu}(q)$. The $q\bar{q}$ blob contains all possible QCD corrections. The dashed vertical line indicates that the blob is cut in all possible ways, so that the left and right sides correspond to the production amplitude T and its complex-conjugate $T^\dagger$, respectively, for a given intermediate state.

175

Well below the Z peak, the hadronic production is dominated by the γ-exchange contribution. Thus, we can compute the cross-sections of all subprocesses $e^+e^- \to \gamma^* \to q\bar{q}, q\bar{q}G, \ldots$ (at a given order in α_s), and make the sum. Technically, it is much easier to compute the QCD T-product of two electromagnetic currents $[J^\mu_{\rm em} = \sum_f Q_f \bar{q}_f \gamma^\mu q_f]$:

$$\Pi^{\mu\nu}(q) \equiv i \int d^4x \, e^{iqx} \, \langle 0|T\left(J^\mu_{\rm em}(x)J^\nu_{\rm em}(0)^\dagger\right)|0\rangle = \left(-g^{\mu\nu}q^2 + q^\mu q^\nu\right) \Pi_{\rm em}(q^2). \tag{5.2}$$

As shown in Fig. 15, the absorptive part of this object (i.e. the imaginary part, which results from cutting –putting *on shell*– the propagators of the intermediate exchanged quarks and gluons in all possible ways) just corresponds to the sum of the squared moduli of the different production amplitudes. The exact relation with the total cross-section is:

$$R_{e^+e^-} \equiv \frac{\sigma(e^+e^- \to {\rm hadrons})}{\sigma(e^+e^- \to \mu^+\mu^-)} = 12\pi \, {\rm Im}\Pi_{\rm em}(s). \tag{5.3}$$

Neglecting the small (away from thresholds) corrections generated by the non-zero quark masses, the ratio $R_{e^+e^-}$ is given by a perturbative series in powers of $\alpha_s(s)$:

$$
\begin{aligned}
R_{e^+e^-} &= \left(\sum_{f=1}^{N_f} Q_f^2\right) N_C \left\{1 + \sum_{n\geq 1} F_n \left(\frac{\alpha_s(s)}{\pi}\right)^n\right\} \\
&= \left(\sum_{f=1}^{N_f} Q_f^2\right) N_C \left\{1 + F_1 \frac{\alpha_s(\mu^2)}{\pi} + \left[F_2 + F_1 \frac{\beta_1}{2}\ln\left(\frac{s}{\mu^2}\right)\right]\left(\frac{\alpha_s(\mu^2)}{\pi}\right)^2 \right. \\
&\quad \left. + \left[F_3 + F_2\beta_1\ln\left(\frac{s}{\mu^2}\right) + F_1\left(\frac{\beta_2}{2}\ln\left(\frac{s}{\mu^2}\right) + \frac{\beta_1^2}{4}\ln^2\left(\frac{s}{\mu^2}\right)\right)\right]\left(\frac{\alpha_s(\mu^2)}{\pi}\right)^3 + \mathcal{O}(\alpha_s^4)\right\}.
\end{aligned} \tag{5.4}
$$

The second expression, shows explicitly how the running coupling $\alpha_s(s)$ sums an infinite number of higher-order logarithmic terms.

So far, the calculation has been performed to order α_s^3, with the result (in the $\overline{MS}$ scheme) [26,27]:

$$
\begin{aligned}
F_1 &= 1, \\
F_2 &= 1.986 - 0.115N_f, \\
F_3 &= -6.637 - 1.200N_f - 0.005N_f^2 - 1.240\frac{\left(\sum_f Q_f\right)^2}{3\sum_f Q_f^2}.
\end{aligned} \tag{5.5}
$$

Note the different charge-dependence on the last term, which is due to the contribution from three intermediate gluons (with a separate quark trace attached to each electromagnetic current in Fig. 15).

For 5 flavours, one has:

$$R_{e^+e^-}(s) = \frac{11}{3}\left\{1 + \frac{\alpha_s(s)}{\pi} + 1.411\left(\frac{\alpha_s(s)}{\pi}\right)^2 - 12.80\left(\frac{\alpha_s(s)}{\pi}\right)^3 + \mathcal{O}(\alpha_s^4)\right\}. \tag{5.6}$$

The perturbative uncertainty of this prediction is of order α_s^4, since the coefficient F_4 is unknown. This uncertainty also includes the ambiguities related to the choice

of renormalization scale and scheme. Although, the total sum of the perturbative series is of course independent of our renormalization conventions, different choices of scale and/or scheme lead to slightly different numerical predictions for the truncated series. For instance, the perturbative series truncated at a finite order N, $R_{e^+e^-}^{(N)}(s) \equiv \left(\sum_f Q_f^2\right) N_C \left\{1 + \sum_{n=1}^N F_n \left(\frac{\alpha_s(s)}{\pi}\right)^n\right\}$, has an explicit scale dependence of order α_s^{N+1}:

$$\frac{dR_{e^+e^-}^{(N)}}{d\mu^2} \sim \left(\frac{\alpha_s(\mu^2)}{\pi}\right)^{N+1}. \qquad (5.7)$$

The numerical values of α_s and the F_n $(n \geq 2)$ coefficients depend on our choice of scheme (also β_n for $n \geq 3$). For instance, at second order[2], the relation between the MS and $\overline{\text{MS}}$ schemes is:

$$\alpha_s^{\text{MS}} = \alpha_s^{\overline{\text{MS}}} \left\{1 + \frac{\beta_1}{2}\left[\ln(4\pi) - \gamma_E\right]\frac{\alpha_s^{\overline{\text{MS}}}}{\pi} + \cdots\right\}, \qquad (5.8)$$

$$F_2^{\text{MS}} = F_2^{\overline{\text{MS}}} - F_1 \frac{\beta_1}{2}\left[\ln(4\pi) - \gamma_E\right] = 7.359 - 0.441 N_f. \qquad (5.9)$$

The difference between both schemes is obviously a higher-order effect. With $N_f = 5$, the MS scheme leads to a second-order coefficient $F_2^{\text{MS}} = 5.156$, which is a factor 3.6 bigger than $F_2^{\overline{\text{MS}}}$. Thus, the perturbative series looks more convergent with the $\overline{\text{MS}}$ choice.

The theoretical prediction for $R_{e^+e^-}(s)$ above the $b\text{-}\bar{b}$ threshold is compared [10] in Fig. 3 with the measured data, taking into account mass-corrections and electroweak (Z-exchange) contributions. The two curves correspond to $\Lambda_{\overline{\text{MS}}}^{(N_f=5)} = 60$ MeV (lower curve) and 250 MeV (upper curve). The rising at large energies is due to the tail of the Z peak. A global fit to all data between 20 and 65 GeV yields [28]

$$\alpha_s(34\,\text{GeV}) = 0.146 \pm 0.030. \qquad (5.10)$$

The hadronic width of the Z boson can be analyzed in the same way:

$$R_Z \equiv \frac{\Gamma(Z \to \text{hadrons})}{\Gamma(Z \to e^+e^-)} = R_Z^{\text{EW}} N_C \left\{1 + \sum_{n \geq 1} \tilde{F}_n \left(\frac{\alpha_s(M_Z^2)}{\pi}\right)^n + \mathcal{O}\left(\frac{m_f^2}{M_Z^2}\right)\right\}. \qquad (5.11)$$

The global factor

$$R_Z^{\text{EW}} = \frac{\sum_f(v_f^2 + a_f^2)}{v_e^2 + a_e^2}(1 + \delta_{\text{EW}}) \qquad (5.12)$$

contains the underlying electroweak $Z \to \sum_f q_f \bar{q}_f$ decay amplitude. Since both vector and axial-vector couplings are present, the QCD-correction coefficients $\tilde{F}_n$ are slightly different from F_n for $n \geq 2$. For instance, the Z axial coupling generates the two-loop contribution $Z \to t\bar{t} \to GG \to q\bar{q}$ (through triangular quark diagrams), which is absent in the vector case; this leads to an additional $\mathcal{O}\left(\alpha_s^2 m_t^2/M_Z^2\right)$ correction.

In order to determine α_s from R_Z, one needs to perform a global analysis of the LEP/SLC data, taking properly into account the higher-order electroweak corrections [29,30]. The latest α_s value reported by the LEP Electroweak Working Group [31] is

$$\alpha_s(M_Z^2) = 0.125 \pm 0.005 \pm 0.002. \qquad (5.13)$$

---

2) Actually, at second order a scheme is completely specified by a single parameter. Thus, scale and scheme dependence is just the same at this order. The relations in Eqs. (5.8) and (5.9) are equivalent to a change of scale: $\mu_{\text{MS}}^2 = (4\pi/e^{\gamma_E})\,\mu_{\overline{\text{MS}}}^2$.

5.2 $\tau^- \rightarrow \nu_\tau + $ hadrons

The calculation of QCD corrections to the inclusive decay of the τ lepton [32–36] looks quite similar from a diagrammatic point of view. One just puts all possible gluon (and $q\bar{q}$) corrections to the basic decay diagram in Fig. 4, and computes the sum

$$\Gamma(\tau^- \rightarrow \nu_\tau + \text{hadrons}) = \Gamma(\tau^- \rightarrow \nu_\tau + q\bar{q}) + \Gamma(\tau^- \rightarrow \nu_\tau + q\bar{q}G) + \Gamma(\tau^- \rightarrow \nu_\tau + q\bar{q}GG) + \cdots \tag{5.14}$$

As in the e^+e^- case, the calculation is more efficiently performed through the two-point-function

$$\Pi_L^{\mu\nu}(q) \equiv i \int d^4x \, e^{iqx} \, \langle 0|T\left(L^\mu(x)L^\nu(0)^\dagger\right)|0\rangle = \left(-g^{\mu\nu}q^2 + q^\mu q^\nu\right)\Pi_L^{(1)}(q^2) + q^\mu q^\nu \, \Pi_L^{(0)}(q^2), \tag{5.15}$$

which involves the T-ordered product of two left-handed currents, $L^\mu = \bar{u}\gamma^\mu(1 - \gamma^5)d_\theta$. This object can be easily visualized through a diagram analogous to Fig. 15, where the photon is replaced by a W^- line and one has a $\tau\nu_\tau$ pair in the external fermionic lines instead of the e^+e^- pair. The precise relation with the ratio R_τ is:

$$R_\tau \equiv \frac{\Gamma(\tau^- \rightarrow \nu_\tau + \text{hadrons})}{\Gamma(\tau^- \rightarrow \nu_\tau e^- \bar{\nu}_e)}$$

$$= 12\pi \int_0^{m_\tau^2} \frac{ds}{m_\tau^2} \left(1 - \frac{s}{m_\tau^2}\right)^2 \left\{\left(1 + 2\frac{s}{m_\tau^2}\right)\text{Im}\Pi_L^{(1)}(s) + \text{Im}\Pi_L^{(0)}(s)\right\}. \tag{5.16}$$

The three-body character of the basic decay mechanism, $\tau^- \rightarrow \nu_\tau u d_\theta$, shows here a crucial difference with e^+e^- annihilation. One needs to integrate over all possible neutrino energies or, equivalently, over all possible values of the total hadronic invariant-mass s. The spectral functions $\text{Im}\Pi_L^{(0,1)}(s)$ contain the dynamical information on the invariant-mass distribution of the final hadrons. The lower integration limit corresponds to the threshold for hadronic production, i.e. m_π (equal to zero for massless quarks). Clearly, this lies deep into the non-perturbative region where confinement is crucial. Thus, it is very difficult to make a reliable prediction for the integrand in (5.16).
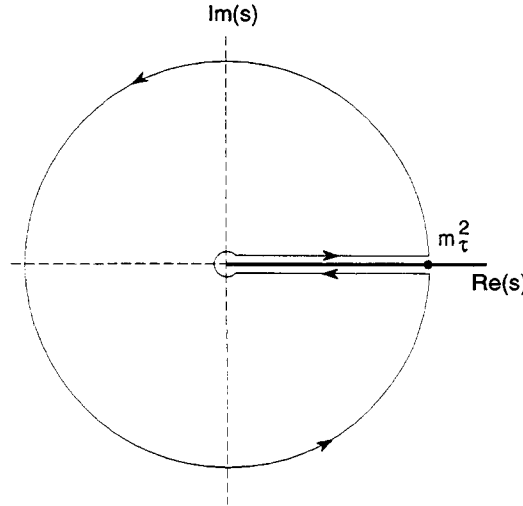

Figure 16: Integration contour in the complex s-plane used to obtain Eq. (5.17).

Fortunately, we have precious exact (i.e. non-perturbative) information on the dynamical functions $\Pi_L^{(0,1)}(s)$, which allows us to accurately predict the total integral

178

(5.16): $\Pi_L^{(0,1)}(s)$ are analytic functions in the complex s-plane except for a cut in the positive real axis. The physics we are interested in lies of course in the singular region, where hadrons are produced. We need to know the integral along the physical cut of $\mathrm{Im}\Pi_L^{(0,1)}(s) = -\frac{i}{2}[\Pi_L^{(0,1)}(s+i\epsilon) - \Pi_L^{(0,1)}(s-i\epsilon)]$. However, we can use Cauchy's theorem (close integrals of analytic functions are zero if there are no singularities within the integration contour), to express R_τ as a contour integral in the complex s-plane running counter-clockwise around the circle $|s| = m_\tau^2$ [32–34]:

$$R_\tau = 6\pi i \oint_{|s|=m_\tau^2} \frac{ds}{m_\tau^2} \left(1 - \frac{s}{m_\tau^2}\right)^2 \left\{ \left(1 + 2\frac{s}{m_\tau^2}\right) \Pi_L^{(0+1)}(s) - 2\frac{s}{m_\tau^2}\Pi_L^{(0)}(s) \right\}. \qquad (5.17)$$

The advantage of this expression is that it requires dynamical information only for complex s of order m_τ^2, which is significantly larger than the scale associated with non-perturbative effects in QCD. A perturbative calculation of R_τ is then possible.

Using the so-called *Operator Product Expansion* techniques it is possible to show [33, 34, 36] that non-perturbative contributions are very suppressed $[\sim (\Lambda/m_\tau)^6]$. Thus, R_τ is a perfect observable for determining the strong coupling. In fact, τ decay is probably the lowest energy process from which the running coupling constant can be extracted cleanly, without hopeless complications from non-perturbative effects. The τ mass, $m_\tau = 1.7771 {}^{+0.0004}_{-0.0005}$ GeV [10], lies fortuitously in a *compromise* region where the coupling constant α_s is large enough that R_τ is very sensitive to its value, yet still small enough that the perturbative expansion still converges well.

The explicit calculation gives [34, 36]:

$$R_\tau = 3\left(|V_{ud}|^2 + |V_{us}|^2\right) S_{\mathrm{EW}} \left\{1 + \delta'_{\mathrm{EW}} + \delta^{(0)} + \delta_{\mathrm{NP}}\right\}, \qquad (5.18)$$

where $S_{\mathrm{EW}} = 1.0194$ and $\delta'_{\mathrm{EW}} = 0.0010$ are the leading and next-to-leading electroweak corrections, and $\delta^{(0)}$ contains the dominant perturbative-QCD contribution:

$$\delta^{(0)} = \frac{\alpha_s(m_\tau^2)}{\pi} + \left[F_2 - \frac{19}{24}\beta_1\right]\left(\frac{\alpha_s(m_\tau^2)}{\pi}\right)^2$$

$$+ \left[F'_3 - \frac{19}{12}F_2\beta_1 - \frac{19}{24}\beta_2 + \frac{265}{288}\beta_1^2\right]\left(\frac{\alpha_s(m_\tau^2)}{\pi}\right)^3 + \mathcal{O}(\alpha_s^4) \qquad (5.19)$$

$$= \frac{\alpha_s(m_\tau^2)}{\pi} + 5.2023\left(\frac{\alpha_s(m_\tau^2)}{\pi}\right)^2 + 26.366\left(\frac{\alpha_s(m_\tau^2)}{\pi}\right)^3 + \mathcal{O}(\alpha_s^4). \qquad (5.20)$$

The remaining factor $\delta_{\mathrm{NP}} \approx -0.016 \pm 0.005$ includes the estimated [34, 36] small mass-corrections and non-perturbative contributions.

Owing to its high sensitivity to α_s [33,34] the ratio R_τ has been a subject of intensive study in recent years. Many different sources of possible perturbative and non-perturbative contributions have been analyzed in detail. Higher-order logarithmic corrections have been resummed [35], leading to very small renormalization-scheme dependences. The size of the non-perturbative contributions has been experimentally analyzed, through a study of the invariant-mass distribution of the final hadrons [37]; the present data implies [38] $\delta_{\mathrm{NP}} = (0.3 \pm 0.5)\%$ confirming the predicted [34] suppression of non-perturbative corrections. An exhaustive summary of the R_τ analysis can be found in Ref. [36].

Using the Particle Data Group values for the τ lifetime and leptonic branching ratios [10], the theoretical analysis of R_τ results in a fitted value of α_s [36],

$$\alpha_s(m_\tau^2) = 0.33 \pm 0.03, \tag{5.21}$$

which is significantly larger than (5.13). After evolution up to the scale M_Z, the strong coupling constant in Eq. (5.21) decreases to $\alpha_s(M_Z^2) = 0.120^{+0.003}_{-0.004}$, in excellent agreement with the Z-width determination and with a smaller error bar. This comparison provides a beautiful test of the predicted running of α_s.

5.3 $e^+e^- \to$ jets
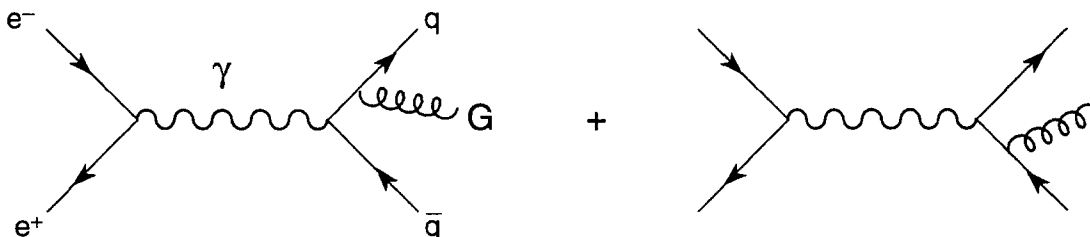

Figure 17: Gluon bremsstrahlung corrections to $e^+e^- \to q\bar{q}$.

At lowest-order in the strong coupling, the hadronic production in e^+e^- collisions proceeds through $e^+e^- \to q\bar{q}$. Thus, at high-energies, the final hadronic states are predicted to have mainly a two-jet structure, which agrees with the empirical observations. At $\mathcal{O}(\alpha_s)$, the emission of a hard gluon from a quark leg generates the $e^+e^- \to q\bar{q}G$ transition, leading to 3-jet configurations. For massless quarks, the differential distribution of the 3-body final state is given by:

$$\frac{1}{\sigma_0} \frac{d^2\sigma}{dx_1 dx_2} = \frac{2\alpha_s}{3\pi} \frac{x_1^2 + x_2^2}{(1-x_1)(1-x_2)}, \tag{5.22}$$

where

$$\sigma_0 \equiv \frac{4\pi\alpha^2}{3s} N_C \sum_{f=1}^{N_f} Q_f^2 \tag{5.23}$$

is the lowest-order $e^+e^- \to \gamma^* \to q\bar{q}$ cross-section. The kinematics is defined through the invariants $s \equiv q^2$ and $s_{ij} \equiv (p_i + p_j)^2 = (q - p_k)^2 \equiv s(1-x_k)$ $(i,j,k=1,2,3)$, where p_1, p_2 and p_3 are the quark, antiquark and gluon momenta, respectively, and q is the total e^+e^- momentum. For given s, there are only two independent kinematical variables since

$$x_1 + x_2 + x_3 = 2. \tag{5.24}$$

In the centre-of-mass system $[q^\mu = (\sqrt{s}, \vec{0})]$, $x_i = E_i/E_e = 2E_i/\sqrt{s}$.

Eq. (5.22) diverges as x_1 or x_2 tend to 1. This is a very different infinity from the ultraviolet ones encountered before in the loop integrals. In the present case, the tree amplitude itself is becoming singular in the phase-space boundary. The problem originates in the infrared behaviour of the intermediate quark propagators:

$$\begin{aligned}
x_1 \to 1 &\iff (p_2 + p_3)^2 = 2(p_2 \cdot p_3) \to 0 \; ; \\
x_2 \to 1 &\iff (p_1 + p_3)^2 = 2(p_1 \cdot p_3) \to 0 \; .
\end{aligned} \tag{5.25}$$

There are two distinct kinematical configurations leading to *infrared divergences*:

1. **Collinear gluon**: The 4-momentum of the gluon is parallel to that of either the quark or the antiquark. This is also called a *mass singularity*, since the divergence would be absent if either the gluon or the quark had a mass ($p_3 \| p_2$ implies $s_{23} = 0$ if $p_2^2 = p_3^3 = 0$).

2. **Soft gluon**: $p_3 \to 0$.

   In either case, the observed final hadrons will be detected as a 2-jet configuration, because the qG or $\bar{q}G$ system cannot be resolved. Owing to the finite resolution of any detector, it is not possible (not even in principle) to separate those 2-jet events generated by the basic $e^+e^- \to q\bar{q}$ process, from $e^+e^- \to q\bar{q}G$ events with a collinear or soft gluon. In order to resolve a 3-jet event, the gluon should have an energy and opening angle (with respect to the quark or antiquark) bigger than the detector resolution. The observable 3-jet cross-section will never include the problematic region $x_{1,2} \to 1$; thus, it will be finite, although its value will depend on the detector resolution and/or the precise definition of *jet* (i.e. σ depends on the chosen integration limits).

   On the other side, the 2-jet configurations will include both $e^+e^- \to q\bar{q}$ and $e^+e^- \to q\bar{q}G$ with an unobserved gluon. The important question is then the infrared behaviour of the sum of both amplitudes. The exchange of virtual gluons among the quarks generate an $\mathcal{O}(\alpha_s)$ correction to the $e^+e^- \to q\bar{q}$ amplitude:

$$T[e^+e^- \to q\bar{q}] = T_0 + T_1 + \cdots \qquad (5.26)$$

where T_0 is the lowest-order (tree-level) contribution, T_1 the $\mathcal{O}(\alpha_s)$ correction, and so on. The interference of T_0 and T_1 gives rise to an $\mathcal{O}(\alpha_s)$ contribution to the $e^+e^- \to q\bar{q}$ cross-section.
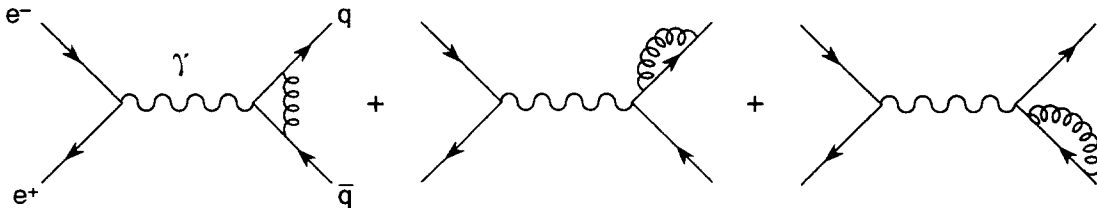

Figure 18: 1-loop gluonic corrections to $e^+e^- \to q\bar{q}$.

We know already that loop diagrams have ultraviolet divergences which must be renormalized. In addition, they also have infrared divergences associated with collinear and soft configurations of the virtual gluon. One can explicitly check that the $\mathcal{O}(\alpha_s)$ infrared divergence of $\sigma(e^+e^- \to q\bar{q})$ exactly cancels the one in $\sigma(e^+e^- \to q\bar{q}G)$, so that the sum is well-defined:

$$\sigma(e^+e^- \to q\bar{q}) + \sigma(e^+e^- \to q\bar{q}G) + \cdots = \sigma_0 \left(1 + \frac{\alpha_s}{\pi} + \cdots \right) . \qquad (5.27)$$

This is precisely the inclusive result discussed in Sect. 5.1. This remarkable cancellation of infrared divergences is actually a general result (Bloch-Nordsieck [39] and Kinoshita–Lee–Nauenberg [40] theorems): for inclusive enough cross-sections both the soft and collinear infrared divergences cancel.

While the total hadronic cross-section is unambiguously defined, we need a precise definition of jet in order to classify a given event as a 2-, 3-, ..., or n-jet configuration.
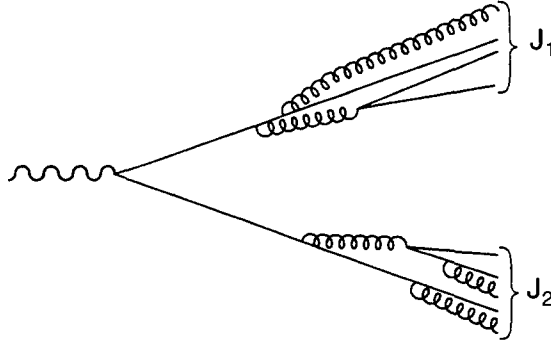
Figure 19: 2-jet configuration.

Such a definition should be free of infrared singularities, and insensitive to the details of the non-perturbative fragmentation into hadrons. A popular example of jet definition is the so-called JADE algorithm [41], which makes use of an invariant-mass cut y:

$$\text{3 jet} \quad \Longleftrightarrow \quad s_{ij} \equiv (p_i + p_j)^2 > ys \qquad (\forall i, j = 1, 2, 3) \ . \tag{5.28}$$

Clearly, both the theoretical predictions and the experimental measurements depend on the adopted jet definition. With the JADE algorithm, the fraction of 3-jet events is predicted to be:

$$R_3 = \frac{2\alpha_s}{3\pi} \left\{ (3-6y) \ln\left(\frac{y}{1-2y}\right) + 2\ln^2\left(\frac{y}{1-y}\right) + \frac{5}{2} - 6y - \frac{9}{2}y^2 + 4\text{Li}_2\left(\frac{y}{1-y}\right) - \frac{\pi^2}{3} \right\}, \tag{5.29}$$

where

$$\text{Li}_2(z) \equiv -\int_0^z \frac{d\xi}{1-\xi} \ln\xi \ . \tag{5.30}$$

The corresponding fraction of 2-jet events is given by $R_2 = 1 - R_3$. The fraction of 2- or 3-jet events obviously depends on the chosen cut y. The infrared singularities are manifest in the divergent behaviour of R_3 for $y \to 0$.

At higher-orders in α_s one needs to define the different multi-jet fractions. For instance, one can easily generalize the JADE algorithm an classify a $\{p_1, p_2, \ldots, p_n\}$ event as a n-jet configuration provided that $s_{ij} > ys$ for all $i, j = 1, \ldots, n$. If a pair of momenta does not satisfy this constraint, they are combined into a single momentum and the event is considered as a $(n-1)$ jet configuration (if the constraint is satisfied by all other combinations of momenta). The general expression for the fraction of n-jet events takes the form:

$$R_n(s, y) = \left(\frac{\alpha_s(s)}{\pi}\right)^{n-2} \sum_{j=0} C_j^{(n)}(y) \left(\frac{\alpha_s(s)}{\pi}\right)^j , \tag{5.31}$$

with $\sum_n R_n = 1$.

A few remarks are in order here:

- The jet fractions have a high sensitivity to α_s $[R_n \sim \alpha_s^{n-2}]$. Although the sensitivity increases with n, the number of events decreases with the jet multiplicity.
- Higher-order $\alpha_s(\mu^2)^j \ln^k(s/\mu^2)$ terms have been summed into $\alpha_s(s)$. However, the coefficients $C_j^{(n)}(y)$ still contain $\ln^k(y)$ terms. At low values of y, the infrared divergence $(y \to 0)$ reappears and the perturbative series becomes unreliable. For large y, the jet fractions R_n with $n \geq 3$ are small.

–   Experiments measure hadrons rather than partons. Therefore, since these observables are not fully inclusive, there is an unavoidable dependence on the non-perturbative fragmentation into hadrons. This is usually modelled through Monte Carlo analyses, and introduces theoretical uncertainties which need to be estimated.

Many different jet algorithms and jet variables (jet rates, event shapes, energy correlations, ...) have been introduced to optimize the perturbative analysis. In some cases, a resummation of $\alpha_s(s)^n \ln^m(y)$ contributions with $m > n$ has been performed to improve the predictions at low y values [42].
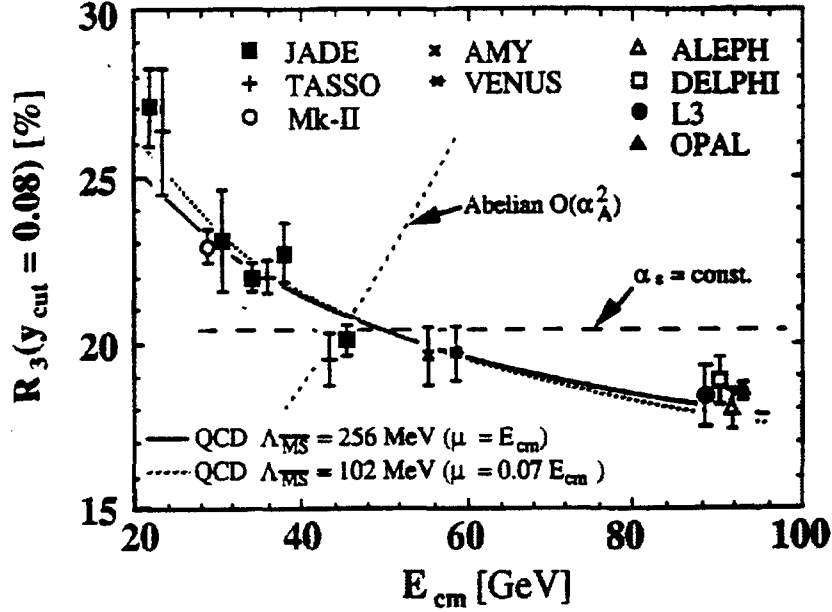

Figure 20: Energy dependence of 3-jet event production rates $R_3(y = 0.8)$, compared with predictions of analytic $\mathcal{O}(\alpha_s^2)$ QCD calculations, with the hypothesis of an energy independent α_s and with the abelian vector theory in $\mathcal{O}(\alpha_A^2)$ (taken from Ref. [43]).

Fig. 20 [43] shows the energy dependence of the measured 3-jet production fraction R_3 ($y = 0.08$), compared with QCD predictions. The data is in good agreement with QCD and fits very well the predicted energy-dependence of the running coupling. A constant value of α_s cannot describe the observed production rates. The figure shows also the predictions obtained with an abelian vector theory at $\mathcal{O}(\alpha_A^2)$, which are clearly excluded.

Several measurements of α_s, using different jet variables, have been performed. All measurements are in good agreement, providing a good consistency test of the QCD predictions. Combining the results from all experiments at LEP and SLC, one gets the average value [7]:

$$\alpha_s(M_Z^2) = \begin{cases} 0.119 \pm 0.006 & (\mathcal{O}(\alpha_s)^2) \\ 0.123 \pm 0.006 & \text{(resummed calculations)} \end{cases} . \qquad (5.32)$$

The two numbers correspond to different theoretical approximations used in the fits to extract α_s.

3-jet events can also be used to test the gluon spin. For a spin-0 gluon, the differential distribution is still given by Eq. (5.22), but changing the $x_1^2 + x_2^2$ factor in the

numerator to $x_3^2/4$. In general, one cannot readily be sure which hadronic jet emerges via fragmentation from a quark (or antiquark), and which from a gluon. Therefore, one adopts instead a jet ordering, $x_1 > x_2 > x_3$, where x_1 refers to the most energetic jet, 2 to the next and 3 to the least energetic one, which most likely would correspond to the gluon. When $x_2 \to 1$ ($x_1 \to 1$) the vector-gluon distribution is singular, but the corresponding scalar-gluon distribution is not because at that point $x_3 = (1 - x_1) + (1 - x_2) \to 0$. The measured distribution agrees very well with the QCD predictions with a spin-1 gluon; a scalar gluon is clearly excluded.
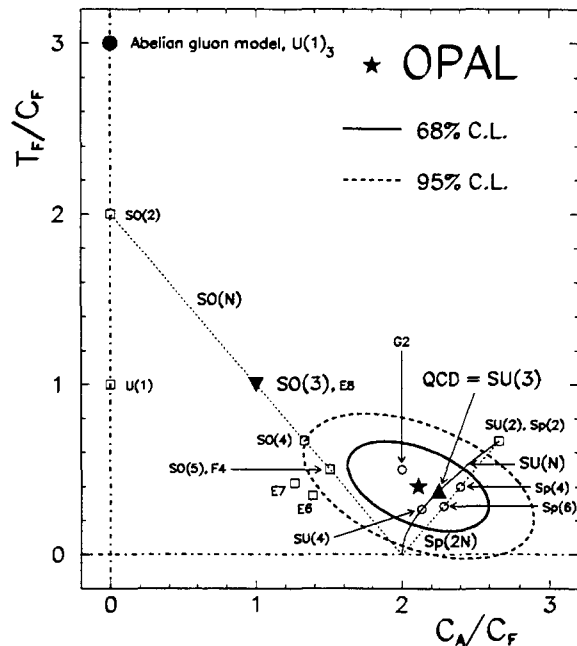

Figure 21: 68% and 95% CL contours in the T_F/C_F versus C_A/C_F plane, from OPAL data [44]. Expectations from various gauge models are also shown.
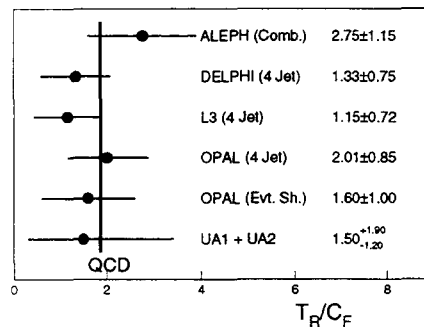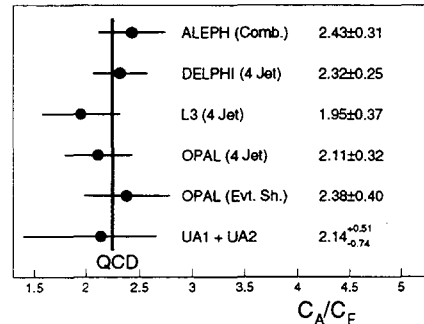

Figure 22: Summary of colour-factor measurements [8]. The results refer to 5 active flavours with $T_R \equiv N_f T_F = 5T_F$.

The predictions for jet distributions and event shapes are functions of the colour-group factors $T_F = 1/2$, $C_F = (N_C^2 - 1)/(2N_C)$ and $C_A = N_C$. These quantities, defined in Eq. (A.5), result from the colour algebra associated with the different interaction vertices, and characterize the colour-symmetry group. If the strong interactions were based on a different gauge group, the resulting predictions would differ in the values of these three factors. Since the vertices contribute in a different way to different observables, these colour factors can be measured by performing a combined fit to the data. Fig. 21 compares a recent OPAL determination [44] of C_A/C_F and T_F/C_F with the values of these two ratios for different colour groups. The data is in excellent agreement with the $SU(3)$ values, and rules out the Abelian model and many classical Lie groups. Notice that those groups shown by the open squares and circles are already excluded because they do not contain three colour degrees of freedom for quarks. Similar results have been presented by the other LEP experiments (the hadronic production of jets at $p\bar{p}$ colliders has also been analyzed in a similar way). A summary of the colour-factor ratios obtained by the different experiments is given in Fig. 22.

6. DEEP INELASTIC SCATTERING

We saw in Section 1.2 how the deep inelastic scattering (DIS) $e^-p \to e^-X$ can be used to learn about the proton structure. Since this involves a bound hadronic state –the proton–, non-perturbative phenomena such as confinement plays here a crucial role. At the same time, the data obeys Bjorken scaling which manifests the asymptotic freedom property of the strong interactions. Thus, DIS appears to be an interesting place where to investigate both perturbative and non-perturbative aspects of QCD.

DIS can be visualized as a two-step process. First, the hard intermediate photon, which is far off its mass-shell, scatters off a quark or gluon with a large momentum transfer; this scattering can be adequately described by perturbation theory. Second, the outgoing partons recombine into hadrons in a time of $\mathcal{O}(1/\Lambda)$. Although this recombination is not calculable in perturbation theory, the details of the non-perturbative hadronization can be avoided, by considering fully inclusive rates, so that perturbative QCD can be applied. However, the hadronic bound-structure of the initial proton state, still introduces a non-perturbative ingredient: the proton structure functions.

6.1   Free parton model

Let us ignore any QCD interactions and let us assume that the nucleon (either proton or neutron) constituents are free spin-$\frac{1}{2}$ partons. Within the quark model, the nucleons have three point-like constituents ($p = u_v u_v d_v$, $n = u_v d_v d_v$), which we will call *valence* quarks. Gluons are of course there; however, they do not interact directly with the photon probe. The photon–gluon interaction only occurs through the virtual q-$\bar{q}$ pairs coupled to the gluon constituents. Thus, instead of gluons, the photon feels a *sea* of q-$\bar{q}$ partons within the nucleon.

Let us denote $u(x)$, $\bar{u}(x)$, $d(x)$, $\bar{d}(x)$, $s(x)$, $\bar{s}(x)$, ... the probability distributions for u, $\bar{u}$, d, $\bar{d}$, s, $\bar{s}$, ... quarks with momentum fraction x in the proton. We have seen in Section 1.2 that, within the parton model, the proton structure functions have a simple form in terms of parton distributions:

$$F_2^{ep}(x)/x = 2F_1^{ep}(x) = \frac{4}{9}\left[u(x) + \bar{u}(x)\right] + \frac{1}{9}\left[d(x) + \bar{d}(x)\right] + \frac{1}{9}\left[s(x) + \bar{s}(x)\right] + \cdots \quad (6.1)$$

The same parton distributions occur in other DIS processes such as $\nu p \to l^- X$ or $\bar{\nu} p \to l^+ X$. However, since the quark couplings of the intermediate bosonic probe (a $W^\pm$ in that case) are not the same, different combinations of these functions are measured:

$$\begin{aligned} F_2^{\nu p}(x)/x = 2F_1^{\nu p}(x) &= 2\left[d(x) + s(x) + \bar{u}(x) + \bar{c}(x) + \cdots\right], \\ F_3^{\nu p}(x) &= 2\left[d(x) + s(x) - \bar{u}(x) - \bar{c}(x) + \cdots\right], \end{aligned}$$

$$\begin{aligned} & \\ F_2^{\bar{\nu} p}(x)/x = 2F_1^{\bar{\nu} p}(x) &= 2\left[u(x) + c(x) + \bar{d}(x) + \bar{s}(x) + \cdots\right], \\ F_3^{\bar{\nu} p}(x) &= 2\left[u(x) + c(x) - \bar{d}(x) - \bar{s}(x) + \cdots\right]. \end{aligned} \quad (6.2)$$

Using isospin symmetry, we can further relate the up- and down-quark distributions in a neutron to the ones in a proton:

$$u^n(x) = d^p(x) \equiv d(x) \; ; \qquad d^n(x) = u^p(x) \equiv u(x) \; ; \quad (6.3)$$

185

the remaining parton distributions being obviously the same. Thus, combining data from different DIS processes, it is possible to obtain separate information on the individual parton distribution functions.

The quark distributions must satisfy some constraints. Since both the proton and the neutron have zero strangeness,

$$\int_0^1 dx\, [s(x) - \bar{s}(x)] = 0 \; . \tag{6.4}$$

Similar relations follow for the heavier flavours $(c, \ldots)$. The proton and neutron electric charges imply two additional sum rules,

$$\int_0^1 dx\, [u(x) - \bar{u}(x)] = 2 \; , \qquad \int_0^1 dx\, [d(x) - \bar{d}(x)] = 1 \; , \tag{6.5}$$

which just give the excess of u and d quarks over antiquarks.

The quark-model concept of valence quarks gives further insight into the nucleon structure. We can decompose the u and d distribution functions into the sum of valence and sea contributions, and take the remaining parton distributions to be pure sea. Since gluons are flavour singlet, one expects the sea to be flavour independent. In this way, the number of independent distributions is reduced to three:

$$
\begin{aligned}
u(x) &= u_v(x) + q_s(x) \; , \\
d(x) &= d_v(x) + q_s(x) \; , \\
\bar{u}(x) &= \bar{d}(x) = s(x) = \bar{s}(x) = \ldots = q_s(x) \; .
\end{aligned}
\tag{6.6}
$$

Within this model, the strangeness sum rule (6.4) is automatically satisfied, while (6.5) imply constraints on the valence-quark distributions alone.

In the analogous situation of quasi-elastic electron–deuterium scattering, the observed structure function shows a narrow peak around $x = \frac{1}{2}$. This is to be expected, since the deuteron has two nucleon constituents with $M_N \approx \frac{1}{2} M_d$ which share the total momentum in equal terms. A simple three-quark model for the nucleon would suggest the existence of a similar peak at $x = \frac{1}{3}$ in the proton and neutron structure functions. However, the distribution shown in Fig. 7 does not show such behaviour. The difference can be easily understood as originating from the parton-sea contributions. Taking the difference between the proton and neutron structure functions, where the contribution from the sea cancels, the data exhibits indeed a broad peak around $x = \frac{1}{3}$.

Our isospin symmetric parton model implies the so-called Gottfried sum rule [45]:

$$\int_0^1 \frac{dx}{x}\, [F_2^{ep}(x) - F_2^{en}(x)] = \frac{1}{3} \int_0^1 dx\, [u_v(x) - d_v(x)] = \frac{1}{3}, \tag{6.7}$$

which is well satisfied by the data. Another interesting quantity is the ratio

$$\frac{F_2^{en}(x)}{F_2^{ep}(x)} = \frac{4 d_v(x) + u_v(x) + \Sigma_{\text{sea}}}{4 u_v(x) + d_v(x) + \Sigma_{\text{sea}}} \; , \tag{6.8}$$

where Σ_{sea} is the total sea contribution. Since all probability distributions must be positive-definite, this ratio should satisfy the bounds $\frac{1}{4} \le F_2^{en}(x)/F_2^{ep}(x) \le 4$, which are

consistent with the data. The measured ratio appears to tend to 1 at small x, indicating that the sea contributions dominate in that region.

The conservation of the total proton momentum implies an important sum rule:

$$\int_0^1 dx\, x\, \left[u(x) + \bar{u}(x) + d(x) + \bar{d}(x) + s(x) + \bar{s}(x) + \cdots\right] = 1 - \epsilon \,, \qquad (6.9)$$

where ϵ is the fraction of momentum that is not carried by quarks. One finds experimentally that $\epsilon \approx \frac{1}{2}$ (at $Q^2 \sim 10$–40 GeV^2), suggesting that about half of the momentum is carried by gluons. This shows the important role of gluons in the proton structure. Although the naive quark model works very well in many cases, it is a too gross simplification as a model of hadrons, at least al large Q^2.

6.2 QCD-improved parton model

At lowest order the DIS process occurs through the hard scattering between the virtual photon (W, or Z) and one constituent parton. The obvious first QCD corrections will be due to real gluon emission by either the initial or final quark. To get rid of infrared divergences, the one-loop virtual gluon contribution should also be taken into account.
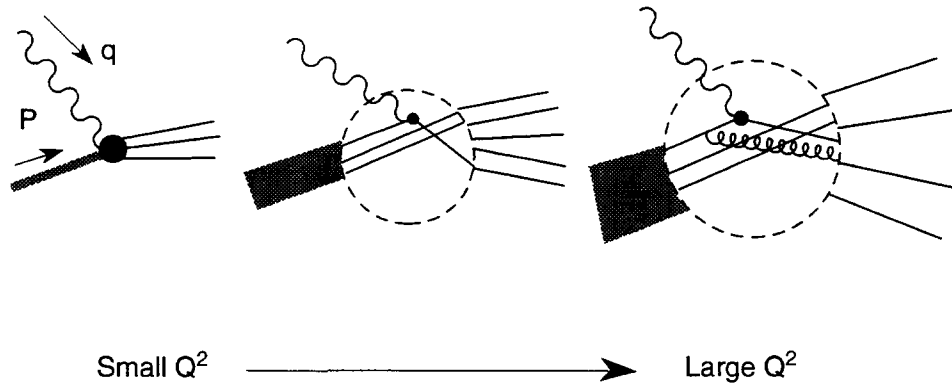

Small Q^2 $\longrightarrow$ Large Q^2

Figure 23: Resolution of the photon probe as function of Q^2.

One can easily understand the main qualitative features of gluon emission, with a few kinematical considerations. At very low values of momentum transfer, the proton behaves as a single object, either point-like (at $Q^2 \approx 0$), or with a finite size. At higher energies, the photon is sensitive to shorter distances and scatters with the constituent partons. Increasing further the momentum transfer, the photon probe has a greater sensitivity to smaller distances, and it is able to resolve the scattered quark into a quark and a gluon. Thus, a parton with momentum fraction x can be resolved into a parton and a gluon of smaller momentum fractions, $x' < x$ and $x - x'$, respectively. In a similar way, a gluon with momentum fraction x can be resolved into a quark and an antiquark.

This simple picture implies that increasing the Q^2, the photon will notice some qualitative changes in the parton distributions:
- Gluon bremsstrahlung will shift the valence and sea distributions to smaller x values.
- The splitting of a gluon into a quark–antiquark pair will increase the amount of sea (mostly at small x).

Thus, without any detailed calculation, one can expect to find a definite Q^2 dependence in the parton distributions; i.e. violations of Bjorken scaling due to the underlying QCD interactions.
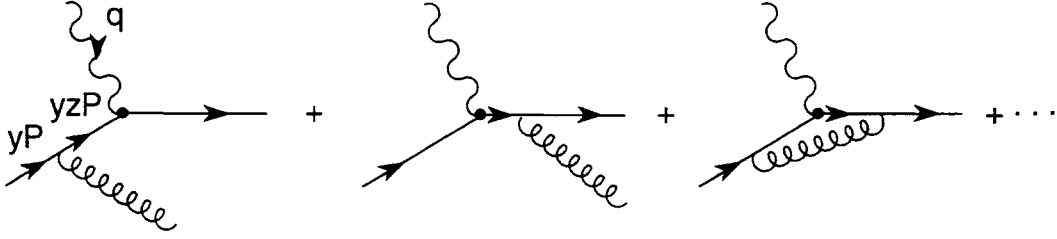
Figure 24: Leading gluonic correction to the basic DIS parton process.

Let us consider a quark with momentum fraction y. At lowest order, its contribution to the proton structure function can be written as

$$2F_1^{(q)}(x) = e_q^2 \int_0^1 dy \, q(y) \, \delta(x - y) \,. \tag{6.10}$$

If the quark emits a gluon before being struck by the photon, its momentum fraction will be degraded to yz $(0 \leq z \leq 1)$. Assuming that the quark remains approximately on-shell, $(q + yzP)^2 \approx m_q^2 \approx 0$, implying that $yz = Q^2/2(P \cdot q) \equiv x$. Therefore, $F_1^{(q)}(x)$ gets contributions from quarks with initial momentum fractions $y \geq x$.

The explicit calculation of the diagrams in Fig. 24 gives the result:

$$2\Delta F_1^{(q)}(x) = e_q^2 \frac{\alpha_s}{2\pi} \int_0^1 dy \, q(y) \int_0^1 dz \, \delta(yz - x) \left\{ P_{qq}^+(z) \ln(Q^2/\nu_{\mathrm{IR}}^2) + C(z) \right\}, \tag{6.11}$$

where

$$P_{qq}(z) \equiv C_F \left(\frac{1 + z^2}{1 - z} \right) \tag{6.12}$$

is called the quark *splitting function*.

The important feature in Eq. (6.11) is the appearance of a *scaling violation* through the logarithmic α_s correction. A careful analysis of the different Feynman diagrams shows that ultraviolet divergences are absent in the total contribution. Therefore, this logarithm has a completely different origin than the ultraviolet ones found in Section 4. The logarithmic behaviour is now generated by infrared singularities of the type discussed in Section 5.3. More precisely, there is a collinear singularity associated with the gluon emission process, which has been regulated with the infrared cut-off ν_{IR}.

The general theorems on the cancellation of infrared divergences do not protect the structure function $F_1^{(q)}(x)$, because this quantity is not *inclusive enough*. The divergence shows up when one tries to resolve the original quark with momentum fraction y into a quark with momentum fraction yz and a gluon. $P_{qq}(z)$ is just the coefficient of the logarithmic divergence associated with the splitting process $q \to qG$. Physical observables should not depend on any cut-off, however, our definition of a parton distribution obviously depends on the power resolution of our photon probe. While at low Q^2 the photon was testing a single parton with momentum fraction $y = x$, now it *feels* the splitting of a quark with $y > x$ into a quark and a gluon with separate parton distributions.

The divergence should then be reabsorbed into the *observable* parton distribution function:

$$q(x, Q^2) = q(x, \nu_{\mathrm{IR}}^2) + \frac{\alpha_s}{2\pi} \ln(Q^2/\nu_{\mathrm{IR}}^2) \int_x^1 \frac{dy}{y} \, q(y) \, P_{qq}^+(x/y) \,. \tag{6.13}$$

Both the *bare* distribution $q(x, \nu_{\text{IR}}^2)$ and the α_s correction depend on the infrared cut-off, but this dependence cancels out and does not show up in the *physical* distribution function[3] $q(x, Q^2)$. Instead, the parton distribution is now a Q^2-dependent quantity, which fits with our intuitive picture that the photon probe increases its resolution power with the scale. In terms of $q(x, Q^2)$, the contribution of the quark q to the proton structure function is given by:

$$2F_1^{(q)}(x) = e_q^2 \left\{ q(x, Q^2) + \frac{\alpha_s}{2\pi} \int_x^1 \frac{dy}{y} \, q(y) \, C\left(x/y\right) \right\}. \qquad (6.14)$$

The individual diagrams in Fig. 24 have also a soft-gluon singularity, which manifests in the divergent behaviour of $P_{qq}(z)$ at $z = 1$. This singularity cancels exactly in the total sum of the gluon-emission and virtual-gluon-exchange contributions. The net result is a slight modification in the definition of the splitting function:

$$P_{qq}^+(z)\,\delta(yz - x) \equiv P_{qq}(z)\,[\delta(yz - x) - \delta(y - x)] \ . \qquad (6.15)$$

Eq. (6.13) shows an important thing: although perturbative QCD is not able to predict the actual value of the distribution function, it does predict how this distribution evolves in $\ln(Q^2)$. Thus, given its value at some reference point Q_0^2, one can compute the quark distribution at any other value of Q^2 (high-enough for perturbation theory to be valid). Including the leading higher-order logarithmic corrections into the running coupling, the Q^2-evolution of the parton distribution is given by [46, 47]:

$$Q^2 \frac{d}{dQ^2} q(x, Q^2) = \frac{\alpha_s(Q^2)}{2\pi} \int_x^1 \frac{dy}{y} \, q(y, Q^2) \, P_{qq}^+(x/y) \ . \qquad (6.16)$$

Thus, the change in the distribution for a quark with momentum fraction x, which interacts with the virtual photon, is given by the integral over y of the corresponding distribution for a quark with momentum fraction $y \geq x$ which, having radiated a gluon, is left with a fraction x/y of its original momentum. The splitting function has then a very intuitive physical interpretation: $(\alpha_s/2\pi)P_{qq}^+(x/y)$ is the probability associated with the splitting process $q(y) \to q(x)G$. This probability is high for large momentum fractions; i.e. high-momentum quarks lose momentum by radiating gluons. Therefore, increasing Q^2, the quark distribution function will decrease at large x and will increase at small x.
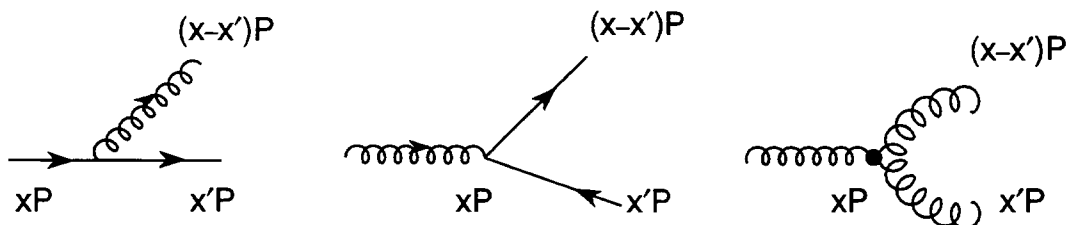

Figure 25: Basic parton-splitting processes.

---

3) Notice, however, that the precise definition of $q(x, Q^2)$ is *factorization-scheme dependent*, since we could always include some arbitrary non-logarithmic α_s correction into $q(x, Q^2)$, by simply shifting the $C\left(x/y\right)$ correction factor in (6.14).

The evolution equation (6.16) is only correct for non-singlet distributions such as $q_i(x) - q_j(x)$, where the (flavour-singlet) gluon contribution cancels out. In general, one needs also to consider the effects coming from the splitting of a gluon into a quark and an antiquark, which interact with the photon probe. The obvious generalization is [47]:

$$Q^2 \frac{d}{dQ^2} \begin{pmatrix} q(x,Q^2) \\ G(x,Q^2) \end{pmatrix} = \frac{\alpha_s(Q^2)}{2\pi} \int_x^1 \frac{dy}{y} \begin{bmatrix} P_{qq}^+(x/y) & P_{qG}(x/y) \\ P_{Gq}(x/y) & P_{GG}(x/y) \end{bmatrix} \begin{pmatrix} q(y,Q^2) \\ G(y,Q^2) \end{pmatrix}, \quad (6.17)$$

where $P_{Gq}(z) = P_{qq}(1-z)$ determines the probability that a quark radiates a gluon with a fraction z of the original quark momentum, while

$$P_{qG}(z) = T_F \left[z^2 + (1-z)^2 \right], \quad (6.18)$$

$$P_{GG}(z) = 2C_A \left[\frac{z}{(1-z)_+} + \frac{1-z}{z} + z(1-z) \right] + \frac{1}{6}(11C_A - 4N_f T_F)\,\delta(1-z), \quad (6.19)$$

are the gluon splitting functions into $q\bar{q}$ and GG, respectively. The subindex "+" in the $1/(1-z)_+$ factor indicates that the $z = 1$ divergence disappears through

$$\int_0^1 dz\, f(z)\,[g(z)]_+ \equiv \int_0^1 dz\,[f(z) - f(1)]\,g(z). \quad (6.20)$$

6.3 Moments of the structure functions

The previous discussion has been based on rather qualitative arguments. Nevertheless, the predicted evolution equation can be derived on a more rigorous basis using the formal framework of the operator product expansion [48], which allows to make a full QCD analysis of the moments

$$M_N^q(Q^2) \equiv \int_0^1 dx\, x^{N-1}\, q(x,Q^2)\,; \qquad M_N^G(Q^2) \equiv \int_0^1 dx\, x^{N-1}\, G(x,Q^2). \quad (6.21)$$

Taking moments on both sides of Eq. (6.17), one finds

$$Q^2 \frac{d}{dQ^2} \begin{pmatrix} M_N^q(Q^2) \\ M_N^G(Q^2) \end{pmatrix} = \frac{\alpha_s(Q^2)}{2\pi} \begin{bmatrix} \gamma_{qq}^N & \gamma_{qG}^N \\ \gamma_{Gq}^N & \gamma_{GG}^N \end{bmatrix} \begin{pmatrix} M_N^q(Q^2) \\ M_N^G(Q^2) \end{pmatrix}, \quad (6.22)$$

where

$$\gamma_{ij}^N \equiv \int_0^1 dz\, z^{N-1}\, P_{ij}(z)\,, \quad (6.23)$$

are the so-called anomalous dimensions. Performing the trivial integrals, one gets:

$$\gamma_{qq}^N = C_F \left[-\frac{1}{2} + \frac{1}{N(N+1)} - 2\sum_{k=2}^N \frac{1}{k} \right],$$

$$\gamma_{qG}^N = T_F \frac{2 + N + N^2}{N(N+1)(N+2)},$$

$$\gamma_{Gq}^N = C_F \frac{2 + N + N^2}{N(N^2 - 1)}, \quad (6.24)$$

$$\gamma_{GG}^N = 2C_A \left[-\frac{1}{12} + \frac{1}{N(N-1)} + \frac{1}{(N+1)(N+2)} - \sum_{k=2}^N \frac{1}{k} \right].$$

For a non-singlet structure function, where the gluon component is absent, the evolution differential equation leads to the solution

$$M_N^{q,\text{ns}}(Q^2) = M_N^{q,\text{ns}}(Q_0^2) \left(\frac{\alpha_s(Q^2)}{\alpha_s(Q_0^2)} \right)^{d_N} ; \qquad d_N \equiv \gamma_{qq}^N / \beta_1 = \frac{-6\gamma_{qq}^N}{33 - 2N_f} . \qquad (6.25)$$

The first moment has $d_1 = 0$; therefore, the Gottfried sum rule (6.7) does not get any QCD correction at this leading order. For $N \geq 2$, $d_N > 0$ so that $M_N^{q,\text{ns}}(Q^2)$ decreases as Q^2 increases, indicating a degradation of momentum in the non-singlet quark distribution.

Let us now consider the flavour-singlet structure function $\Sigma(x) \equiv \sum_i [q_i(x) + \bar{q}_i(x)]$. The $N = 2$ moments $M_2^\Sigma(Q^2)$ and $M_2^G(Q^2)$ give the average total fraction of momentum carried by quarks and gluons, respectively. The corresponding coupled evolution equations can be easily solved. The sum of both moments does not depend on Q^2, since the total momentum is conserved:

$$M_2^\Sigma(Q^2) + M_2^G(Q^2) = 1 . \qquad (6.26)$$

The evolution of the $N = 2$ singlet distribution then takes the simple form

$$\frac{M_2^\Sigma(Q^2) - \frac{N_f}{4C_F} M_2^G(Q^2)}{M_2^\Sigma(Q_0^2) - \frac{N_f}{4C_F} M_2^G(Q_0^2)} = \frac{M_2^\Sigma(Q^2) - \frac{3N_f}{16+3N_f}}{M_2^\Sigma(Q_0^2) - \frac{3N_f}{16+3N_f}} = \left(\frac{\alpha_s(Q^2)}{\alpha_s(Q_0^2)} \right)^{d_2^\Sigma} ; \qquad (6.27)$$

with $d_2^\Sigma = 2(4C_F + N_f)/(33 - 2N_f)$. If $N_f < 16$, $d_2^\Sigma > 0$ and the right-hand side will decrease for increasing Q^2. Thus, one gets a prediction for the asymptotic values of the average total momentum carried by quarks and gluons:

$$\lim_{Q^2 \to \infty} M_2^\Sigma(Q^2) = \frac{3N_f}{16 + 3N_f} ; \qquad \lim_{Q^2 \to \infty} M_2^G(Q^2) = \frac{16}{16 + 3N_f} . \qquad (6.28)$$

For $N_f = 4$, this gives $\frac{3}{7}$ and $\frac{4}{7}$, in good agreement with the empirical observation that for Q^2 in the range 10-40 GeV^2 each fraction is very close to $\frac{1}{2}$.

A very interesting issue is the behaviour of the parton distributions at the endpoints $x = 0$ and $x = 1$. The large N moments probe the $x \to 1$ region, while the low x behaviour is controlled by the $N \to 1$ limit. As N increases, γ_{qG}^N and γ_{Gq}^N tend to zero, so that the evolution equations (6.22) decouple; i.e. the large x behaviour of the quarks is independent of the gluon evolution. When $x \to 1$ the gluon distribution function approach zero more rapidly than the quark ones. For large values of x the quark content of the nucleon is the relevant one. Notice that $x = 1$ means $W^2 = M_p^2$, i.e. it actually corresponds to the elastic photon–nucleon scattering.

At low x, $x/y \to 0$ and the splitting functions $P_{GG}(x/y)$ and $P_{Gq}(x/y)$ diverge. The gluon distribution function becomes then dominant. The low x behaviour is controlled by the singular $N \to 1$ limit of the gluon anomalous dimension $\gamma_{GG}^N \sim 2C_A/(N - 1)$. Making a saddle-point approximation, the $N \to 1$ moment can be inverted; one finds in this way that for low x the gluon distribution function behaves as

$$G(x) \sim \frac{1}{x} \exp \sqrt{C(Q^2) \ln \frac{1}{x}} , \qquad (6.29)$$

with $C(Q^2)$ a calculable function. Obviously, this behaviour cannot be true for arbitrarily small x; something must stop the growing of the gluon distribution before running into unitarity problems.
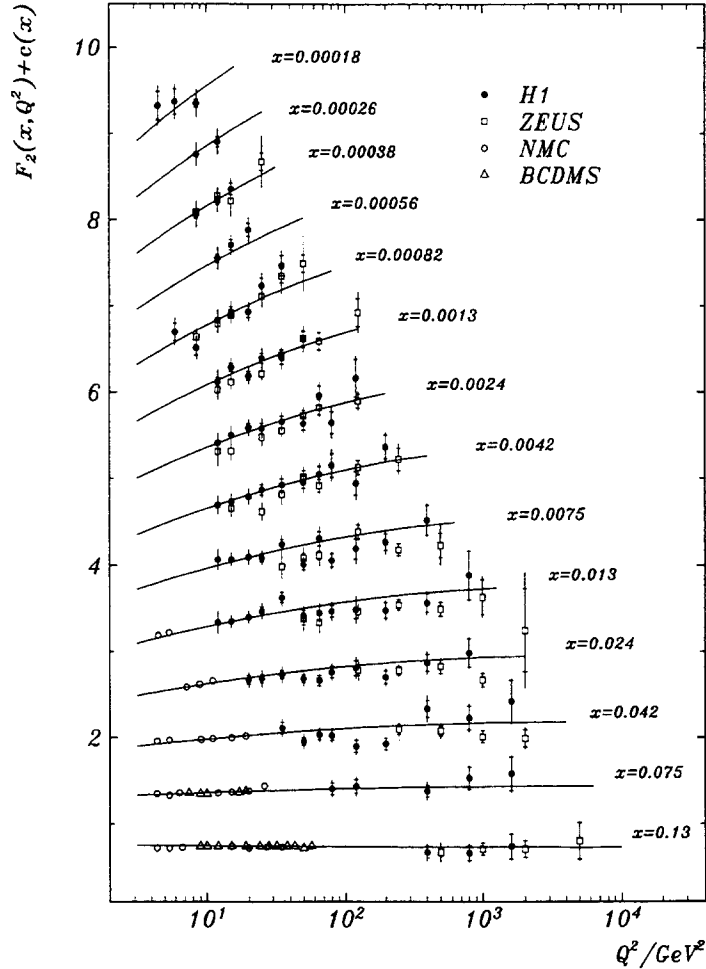
191

Figure 26: Recent measurements of $F_2^{ep}(x, Q^2)$ [49–52]. The $F_2^{ep}(x, Q^2)$ values are plotted with all but normalization errors in a linear scale adding a term $c(x) = 0.6(i_x - 0.4)$ to F_2, where i_x is the bin number starting at $i_x = 1$ for $x = 0.13$. The curves represent a phenomenological fit to the data. (Taken from Ref. [49]).

Kinematically, low x means the high-energy (high W^2) limit for the virtual photon-nucleon scattering. The e-p HERA collider is ideally suited for studying this region. The HERA experiments extend the previously accessible kinematic range up to very large squared momentum transfers, $Q^2 > 5 \times 10^4$ GeV^2, and to very small values of $x < 10^{-4}$. The measurements reported so far [49,50] observe indeed a significant rise of the structure function $F_2^{ep}(x, Q^2)$ with decreasing x, at fixed Q^2. Around $x \sim 10^{-3}$ the decrease of x by an order of magnitude amounts to a rise of $F_2^{ep}(x, Q^2)$ of about a factor of two. The observed Q^2 behaviour is consistent with the expected scaling violations, i.e. a weak rise of $F_2^{ep}(x, Q^2)$ with increasing Q^2 for $x < 0.1$. The most recent data [49–52] on the proton structure function $F_2^{ep}(x, Q^2)$ are shown in Figs. 26 and 27.

6.4 QCD fits to DIS data

There is a twofold motivation for making careful analyses of DIS data. First, the experimental measurement of the parton distributions provides very valuable informa-
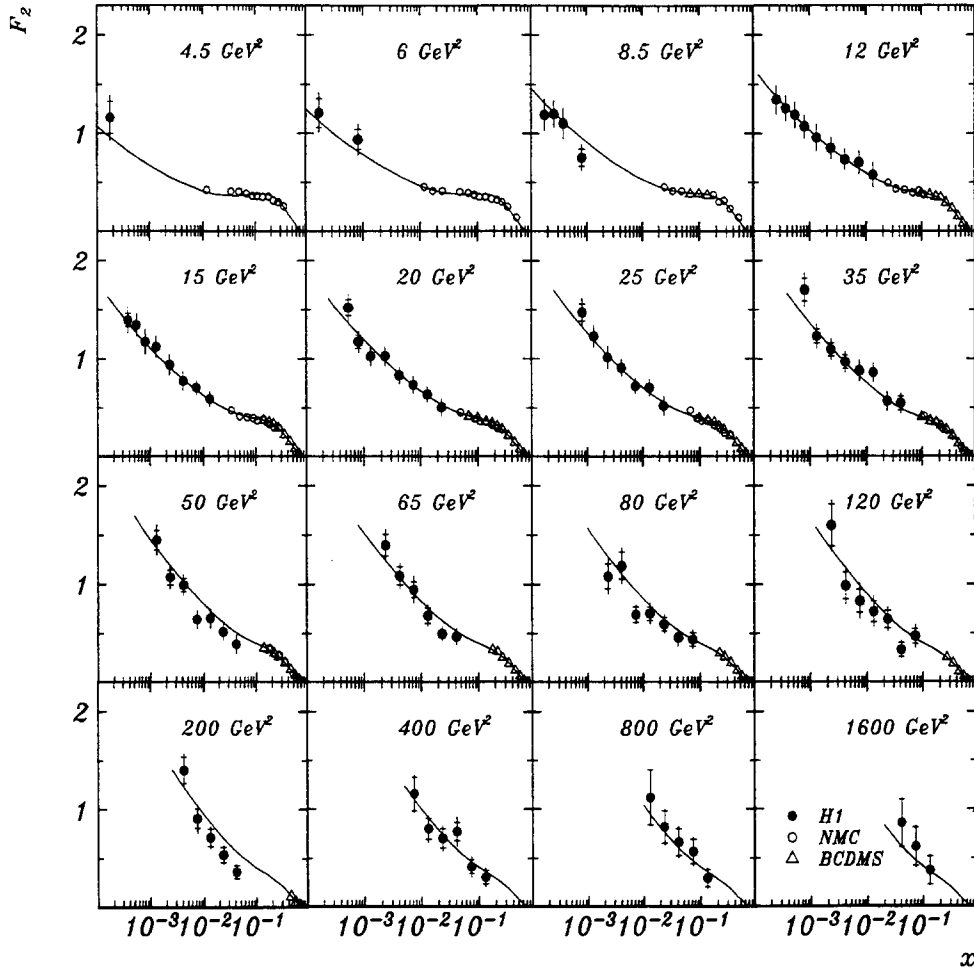
Figure 27: x dependence of the measured structure function $F_2^{ep}(x, Q^2)$, for different Q^2 values [49, 51, 52]. The curves represent a phenomenological fit to the data. (Taken from Ref. [49]).

tion on the non-perturbative regime of the strong interactions (in addition, these parton distributions are needed for making predictions of hard-scattering processes in hadronic collisions). Second, the measured Q^2 evolution (the slopes of the distributions) can be compared with perturbative QCD predictions.

Usually, one adopts some motivated parametrization of the quark and gluon distributions at a fixed momentum-transfer Q_0^2. The evolution equations are then used to get the proton (or neutron) structure functions at arbitrary values of Q^2, and a global fit to the data is performed.

In the actual analysis one needs to worry about the unavoidable presence of additional non-perturbative contributions. The perturbative evolution equations can only predict the leading logarithmic dependence of the distribution functions with Q^2. These distributions have in addition uncalculable non-perturbative corrections suppressed by inverse powers of Q^2, the so-called *higher-twist* contributions:

$$F_i(x, Q^2) = F_i^{\text{LT}}(x, Q^2) + \frac{F_i^{\text{HT}}(x, Q^2)}{Q^2} + \cdots \qquad (6.30)$$

The leading-twist term (LT) is the one predicted by perturbative QCD. Since the ad-

193

ditional $1/(Q^2)^n$ dependences have to be fitted from the data, they increase the final uncertainties. These corrections are numerically important for $Q^2 < \mathcal{O}(10 \text{ GeV}^2)$ and for x close to 1. Obviously, the perturbative QCD predictions can be better tested at large Q^2, where the higher-twist effects are smaller.

Since the singlet structure functions are sensitive to the gluon distribution, which is badly known, they suffer from rather large errors. Good data at low values of x is needed in order to perform an accurate determination. The HERA experiments are making an important improvement in the knowledge of these distributions. The latest fits [53], including the most recent HERA data, obtain gluon and sea-quark distributions at small x which are significantly different from those in previous standard sets of parton distributions. The new gluon distribution is larger for $x \leq 0.01$ and smaller for $x \sim 0.1$. The reduction of the gluon distribution in the interval $x \sim 0.1 - 0.2$ is compensated by an increase in the fitted value of α_s [53], bringing the DIS determination [53,54]

$$\alpha_s(M_Z^2) = 0.114 \pm 0.005 \tag{6.31}$$

in better agreement with the world average values, which we discuss in the next section.

7. DETERMINATION OF THE STRONG COUPLING

In the massless quark limit, QCD has only one free parameter: the strong coupling α_s. Thus, all strong interaction phenomena should be described in terms of this single input. The measurements of α_s at different processes and at different mass scales provide then a crucial test of QCD: if QCD is the right theory of the strong interactions, all measured observables should lead to the same coupling.
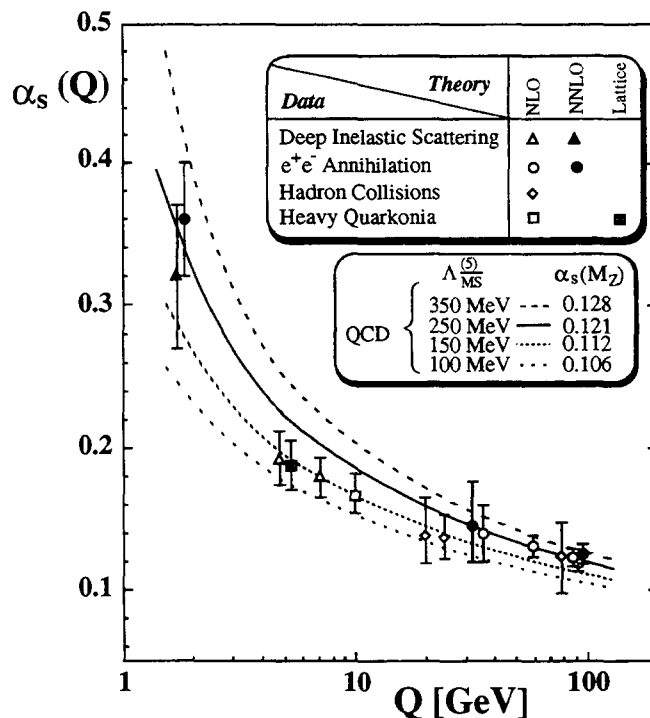

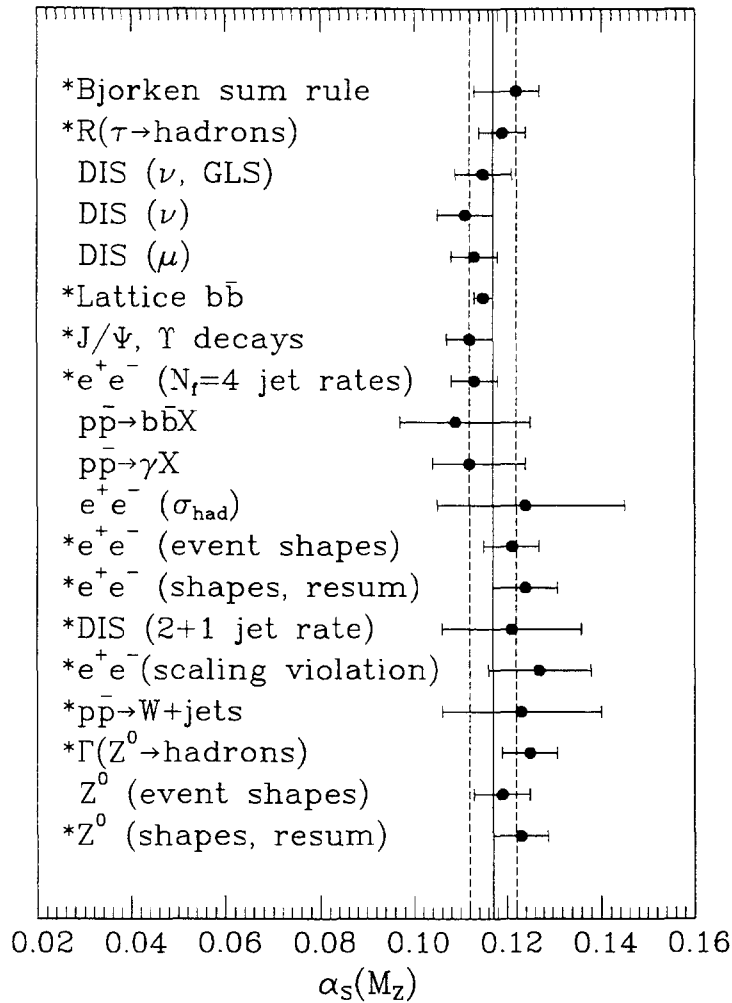Figure 28: Compilation of α_s measurements as function of the energy scale [7,8].

Figure 29: Summary [8] of α_s measurements, evolved to the scale M_Z. Starred items include preliminary results.

Obviously, the test should be restricted to those processes where perturbative techniques are reliable. Moreover, the same definition of α_s should be taken everywhere; the $\overline{\text{MS}}$ scheme is usually adopted as the standard convention. Since the running coupling is a function of energy, one can either compare the different determinations at the different scales where they are measured, checking in this way the predicted Q^2 dependence of the coupling, or use this prediction to bring all measurements to a common reference scale where they are compared. Nowadays, the Z-mass scale is conventionally chosen for such a comparison.

In order to assess the significance of the test, it is very important to have a good understanding of the uncertainties associated with the different measurements. This is not an easy question, because small non-perturbative effects can be present in many observables. In addition, some quantities have been computed to a very good perturbative accuracy (next-to-next-to-leading order), while others are only known at the leading or next-to-leading order; the resulting values of α_s refer then to different perturbative approximations. The estimate of theoretical uncertainties is also affected by the plausible asymptotic (i.e. not convergent) behaviour of the perturbative series in powers of α_s. Although this is a common problem of Quantum Field Theories, it is probably more severe

in QCD because the coupling is rather big (at usual energies).

Fig. 28 summarizes [7,8] the most reliable measurements of the strong coupling as function of the energy scale. The agreement with the predicted running of α_s, indicated by the curves, is indeed very good. The value of $\alpha_s(m_\tau^2)$, extracted from the hadronic width of the τ lepton, provides a very important low-energy measurement; although it has a rather large relative error, it implies a very precise prediction at the M_Z scale, which is in excellent agreement with the direct determinations of $\alpha_s(M_Z^2)$ performed at the Z peak. Fig. 29 [8] compares the different measurements at the common reference scale M_Z. The average af all determinations gives [7,8]:

$$\alpha_s(M_Z^2) = 0.117 \pm 0.005. \tag{7.1}$$

8. CHIRAL SYMMETRY

Up to now, we have only discussed those aspects of QCD which can be analyzed in a perturbative way. Thus, we have restricted ourselves to the study of scattering processes at large momentum transfers, and inclusive transitions which avoid the hadronization problems. The rich variety of strong-interacting phenomena governed by the confinement regime of QCD has been completely ignored.

There are certainly many approximate tools to investigate particular aspects of non-perturbative physics; however, rigorous first-principle QCD calculations seem unfortunately out of reach for present techniques. Nevertheless, we can still investigate some general properties of QCD using symmetry considerations.

8.1 Flavour symmetries

In order to build the QCD Lagrangian, we made extensive use of the $SU(3)_C$ colour symmetry, which is the basis of the strong interaction dynamics. The Lagrangian (3.11) has additional *global* symmetries associated with the quark flavour numbers:

1. $\mathcal{L}_{\text{QCD}}$ is invariant under a global phase redefinition of all quark flavours,

$$q_f \longrightarrow \exp(i\theta)\, q_f \; . \tag{8.1}$$

This symmetry is associated with the conservation of the baryon number.

2. $\mathcal{L}_{\text{QCD}}$ is also invariant under independent phase redefinitions of the different quark flavours,

$$q_f \longrightarrow \exp(i\theta_f)\, q_f \; . \tag{8.2}$$

This symmetry implies the conservation of flavour.

3. For equal quark masses, there is a larger symmetry under $SU(N_f)$ transformations in flavour space,

$$q_f \longrightarrow U_{ff'}\, q_{f'} \; , \qquad\qquad U \in SU(N_f) \; . \tag{8.3}$$

This is a good symmetry of the light-flavour sector (u, d, s), where quark masses can be ignored in first approximation. One has then the well-known isospin $(N_f = 2)$ and $SU(3)$ symmetries.

4. In the absence of quark masses, the QCD Lagrangian splits into two independent quark sectors,

$$\mathcal{L}_{\text{QCD}} \equiv -\frac{1}{4}\, G_a^{\mu\nu} G_{\mu\nu}^a + i\bar{q}_L\gamma^\mu D_\mu q_L + i\bar{q}_R\gamma^\mu D_\mu q_R \; . \tag{8.4}$$

Here, q denotes the flavour (and colour) vector $q = \text{column}(u, d, \dots)$, and L, R stand for the left- and right-handed components of the quarks. Thus, the two quark chiralities live in separate flavour spaces which do not talk each other (gluon interactions do not change the chirality), implying that all previous flavour symmetries get duplicated in the two chiral sectors.

The baryon number symmetry (8.1) is usually called $U(1)_V$, since both chiralities transform in the same way. Its chiral replication is the corresponding $U(1)_A$ transformation:

$$q_L \longrightarrow \exp(-i\theta)\, q_L \; ; \qquad q_R \longrightarrow \exp(i\theta)\, q_R \; . \qquad (8.5)$$

This symmetry of the classical (massless) QCD Lagrangian gets broken by quantum effects (triangular loops of the type shown in Fig. 5, with gluons instead of photons); this is the so-called $U(1)_A$ anomaly. Although (8.5) is not a true symmetry of QCD, it gets broken in a very specific way, which leads to important implications. A discussion of the phenomenological role of anomalies is beyond the scope of these lectures. However, let me mention that this anomaly is deeply related to interesting low-energy phenomena such as the understanding of the η' mass, or the so-called *proton spin crisis*[4].

I want to concentrate here in the chiral extension of the old eightfold $SU(3)_V$ symmetry, i.e. in the global $G \equiv SU(3)_L \otimes SU(3)_R$ symmetry of the QCD Lagrangian for massless u, d and s quarks. This larger symmetry is not directly seen in the hadronic spectrum. Although hadrons can be nicely classified in $SU(3)_V$ representations, degenerate multiplets with opposite parity do not exist. Moreover, the octet of pseudoscalar mesons (π, K, η) happens to be much lighter than all other hadronic states.

There are two different ways in which a symmetry of the Lagrangian can be realized. In the usual one (Wigner–Weyl), the ground state (the vacuum) is also invariant. Then, all physical states can be classified in irreducible representations of the symmetry group [55]. Certainly, the hadronic spectrum does not look like that, in the case of the chiral group.

There is a second (Nambu–Golstone), more sophisticated, way to realize a symmetry. In some cases, the vacuum is not symmetric. The hadronic spectrum corresponds to energy excitations over the physical vacuum and, therefore, will not manifest the original symmetry of the Lagrangian. However, Goldstone's theorem [56] says that in such a case there should appear a massless scalar for each broken generator of the original symmetry group. If the chiral symmetry is realized in this way, there should be eight pseudoscalar massless states (Goldstone bosons) in the hadronic spectrum; this is precisely the number of states of the lightest hadronic multiplet: the 0^- octet. Thus, we can identify the π, K and η with the Goldstone modes of QCD; their small masses being generated by the quark-mass matrix which explicitly breaks the global chiral symmetry of the Lagrangian.

In the Standard electroweak model, the local $SU(2)_L \otimes U(1)_Y$ symmetry is also realized in the Nambu–Goldstone way. There, the symmetry-breaking phenomena is assumed to be related to the existence of some scalar multiplet which gets a vacuum expectation value. Since a *local* symmetry gets (spontaneously) broken in that case, the Goldstone

---

4) This is a quite unfortunate name, because: 1) the underlying QCD dynamics has little to do with the parton-model description of the proton spin; and 2) it is certainly not a crisis but rather a success of QCD. The failure of the naive quark-model description of an observable where gluons are predicted to play a crucial role (the anomaly), is indeed a clear experimental confirmation of the QCD dynamics.

modes combine with the gauge bosons giving massive spin-1 states plus the Higgs particle. The QCD case is simpler, because it is a *global* symmetry the one which gets broken. However, something should play the role of the electroweak scalar field. Since quarks are the only fields carrying flavour, they should be responsible for the symmetry breaking. The simplest possibility is the appearance of a quark condensate

$$v \equiv \langle 0|\bar{u}u|0\rangle = \langle 0|\bar{d}d|0\rangle = \langle 0|\bar{s}s|0\rangle < 0 \ , \tag{8.6}$$

generated by the non-perturbative QCD dynamics. This would produce a dynamical breaking of chiral symmetry, keeping at the same time the observed $SU(3)_V$ symmetry.

8.2 Effective Chiral Lagrangian

The Goldstone nature of the pseudoscalar mesons implies strong constraints on their interactions, which can be most easily analyzed on the basis of an effective Lagrangian. The Goldstone bosons correspond to the zero-energy excitations over the quark condensate; their fields can be collected in a 3×3 unitary matrix $U(\phi)$,

$$\langle 0|\bar{q}_L^j q_R^i|0\rangle \longrightarrow \frac{v}{2} U^{ij}(\phi), \tag{8.7}$$

which parametrizes those excitations. A convenient parametrization is given by

$$U(\phi) \equiv \exp\left(i\sqrt{2}\Phi/f\right), \tag{8.8}$$

where

$$\Phi(x) \equiv \frac{\vec{\lambda}}{\sqrt{2}} \vec{\phi} = \begin{pmatrix} \frac{\pi^0}{\sqrt{2}} + \frac{\eta_8}{\sqrt{6}} & \pi^+ & K^+ \\ \pi^- & -\frac{\pi^0}{\sqrt{2}} + \frac{\eta_8}{\sqrt{6}} & K^0 \\ K^- & \bar{K}^0 & -\frac{2\eta_8}{\sqrt{6}} \end{pmatrix}. \tag{8.9}$$

The matrix $U(\phi)$ transforms linearly under the chiral group, $[g_{L,R} \in SU(3)_{L,R}]$

$$q_L \xrightarrow{G} g_L\, q_L, \quad q_R \xrightarrow{G} g_R\, q_R \quad \Longrightarrow \quad U(\phi) \xrightarrow{G} g_R\, U(\phi)\, g_L^\dagger \ , \tag{8.10}$$

but the induced transformation on the Goldstone fields $\vec{\phi}$ is highly non-linear.

Since there is a mass gap separating the pseudoscalar octet from the rest of the hadronic spectrum, we can build a low-energy effective field theory containing only the Goldstone modes. We should write the most general Lagrangian involving the matrix $U(\phi)$, which is consistent with chiral symmetry. Moreover, we can organize the Lagrangian in terms of increasing powers of momentum or, equivalently, in terms of an increasing number of derivatives (parity conservation requires an even number of derivatives):

$$\mathcal{L}_{\text{eff}}(U) = \sum_n \mathcal{L}_{2n} \ . \tag{8.11}$$

In the low-energy domain, the terms with a minimum number of derivatives will dominate.

Due to the unitarity of the U matrix, $UU^\dagger = 1$, at least two derivatives are required to generate a non-trivial interaction. To lowest order, the effective chiral Lagrangian is uniquely given by the term

$$\mathcal{L}_2 = \frac{f^2}{4} \text{Tr} \left[\partial_\mu U^\dagger \partial^\mu U\right] . \tag{8.12}$$

Expanding $U(\phi)$ in a power series in Φ, one obtains the Goldstone's kinetic terms plus a tower of interactions involving an increasing number of pseudoscalars. The requirement that the kinetic terms are properly normalized fixes the global coefficient $f^2/4$ in (8.12). All interactions among the Goldstones can then be predicted in terms of the single coupling f:

$$\mathcal{L}_2 = \frac{1}{2} \, \text{Tr} \left[\partial_\mu \Phi \partial^\mu \Phi \right] + \frac{1}{12 f^2} \, \text{Tr} \left[(\Phi \overset{\leftrightarrow}{\partial_\mu} \Phi)(\Phi \overset{\leftrightarrow}{\partial^\mu} \Phi) \right] + \mathcal{O}(\Phi^6/f^4). \tag{8.13}$$

To compute the $\pi\pi$ scattering amplitude, for instance, is now a trivial perturbative exercise. One gets the well-known [57] Weinberg result $[t \equiv (p'_+ - p_+)^2]$

$$T(\pi^+ \pi^0 \to \pi^+ \pi^0) = t/f^2. \tag{8.14}$$

Similar results can be obtained for $\pi\pi \to 4\pi, 6\pi, 8\pi, \dots$ The non-linearity of the effective Lagrangian relates amplitudes with different numbers of Goldstone bosons, allowing for absolute predictions in terms of f. Notice that the Goldstone interactions are proportional to their momenta (derivative couplings). Thus, in the zero-momentum limit, pions become free. In spite of confinement, QCD has a weakly-interacting regime at low energies, where a perturbative expansion in powers of momenta can be applied.

It is straightforward to generalize the effective Lagrangian (8.12) to incorporate electromagnetic and semileptonic weak interactions. One learns then that f is in fact the pion-decay constant $f \approx f_\pi = 92.4$ MeV, measured in $\pi \to \mu \nu_\mu$ decay [58]. The corrections induced by the non-zero quark masses are taken into account through the term

$$\mathcal{L}_m = \frac{|v|}{2} \, \text{Tr} \left[\mathcal{M}(U + U^\dagger) \right] \, , \qquad \mathcal{M} \equiv \text{diag}(m_u, m_d, m_s) \, , \tag{8.15}$$

which breaks chiral symmetry in exactly the same way as the quark-mass term in the underlying QCD Lagrangian does. Eq. (8.15) gives rise to a quadratic pseudoscalar-mass term plus additional interactions proportional to the quark masses. Expanding in powers of Φ (and dropping an irrelevant constant), one has

$$\mathcal{L}_m = |v| \left\{ -\frac{1}{f^2} \text{Tr} \left[\mathcal{M} \Phi^2 \right] + \frac{1}{6 f^4} \text{Tr} \left[\mathcal{M} \Phi^4 \right] + \mathcal{O}(\Phi^6/f^6) \right\}. \tag{8.16}$$

The explicit evaluation of the trace in the quadratic mass term provides the relation between the physical meson masses and the quark masses:

$$\begin{aligned}
M^2_{\pi^\pm} &= (m_u + m_d) \frac{|v|}{f^2} \, , \\[4pt]
M^2_{\pi^0} &= (m_u + m_d) \frac{|v|}{f^2} - \varepsilon + \mathcal{O}(\varepsilon^2) \, , \\[4pt]
M^2_{K^\pm} &= (m_u + m_s) \frac{|v|}{f^2} \, , \\[4pt]
M^2_{K^0} &= (m_d + m_s) \frac{|v|}{f^2} \, , \\[4pt]
M^2_{\eta_8} &= \frac{1}{3}(m_u + m_d + 4 m_s) \frac{|v|}{f^2} + \varepsilon + \mathcal{O}(\varepsilon^2) \, ,
\end{aligned} \tag{8.17}$$

where

$$\varepsilon = \frac{|v|}{2f^2} \frac{(m_u - m_d)^2}{(2m_s - m_u - m_d)} \ .$$ (8.18)

Chiral symmetry relates the magnitude of the meson and quark masses to the size of the quark condensate. Taking out the common $|v|/f^2$ factor, Eqs. (8.17) imply the old Current Algebra mass ratios,

$$\frac{M_{\pi^\pm}^2}{m_u + m_d} = \frac{M_{K^+}^2}{(m_u + m_s)} = \frac{M_{K^0}}{(m_d + m_s)} \approx \frac{3M_{\eta_8}^2}{(m_u + m_d + 4m_s)} \ ,$$ (8.19)

and [up to $\mathcal{O}(m_u - m_d)$ corrections] the Gell-Mann–Okubo mass relation

$$3M_{\eta_8}^2 = 4M_K^2 - M_\pi^2 \ .$$ (8.20)

Although chiral symmetry alone cannot fix the absolute values of the quark masses, it gives information about quark-mass ratios. Neglecting the tiny $\mathcal{O}(\varepsilon)$ effects, one gets the relations

$$\frac{m_d - m_u}{m_d + m_u} = \frac{(M_{K^0}^2 - M_{K^+}^2) - (M_{\pi^0}^2 - M_{\pi^+}^2)}{M_{\pi^0}^2} = 0.29 \ ,$$ (8.21)

$$\frac{2m_s - m_u - m_d}{2(m_u + m_d)} = \frac{M_{K^0}^2 - M_{\pi^0}^2}{M_{\pi^0}^2} = 12.6 \ .$$ (8.22)

In (8.21) we have subtracted the pion square-mass difference, to take into account the electromagnetic contribution to the pseudoscalar-meson self-energies; in the chiral limit $(m_u = m_d = m_s = 0)$, this contribution is proportional to the square of the meson charge and it is the same for K^+ and π^+. The mass formulae (8.21) and (8.22) imply the quark-mass ratios advocated by Weinberg:

$$m_u : m_d : m_s = 0.55 : 1 : 20.3 \ .$$ (8.23)

Quark-mass corrections are therefore dominated by m_s, which is large compared with m_u and m_d. Notice that the difference $m_d - m_u$ is not small compared with the individual up- and down-quark masses; in spite of that, isospin turns out to be an extremely good symmetry, because isospin-breaking effects are governed by the small ratio $(m_d - m_u)/m_s$.

The Φ^4 interactions in (8.16) introduce mass corrections to the $\pi\pi$ scattering amplitude (8.14),

$$T(\pi^+\pi^0 \to \pi^+\pi^0) = \frac{t - M_\pi^2}{f_\pi^2} \ .$$ (8.24)

Since $f \approx f_\pi$ is fixed from pion decay, this result is now an absolute prediction of chiral symmetry.

The lowest-order chiral Lagrangian encodes in a very compact way all the Current Algebra results obtained in the sixties [59]. The nice feature of the chiral approach is its elegant simplicity, which allows to estimate higher-order corrections in a systematic way. A detailed summary of the chiral techniques and their phenomenological applications can be found in Ref. [58].

9. SUMMARY

Strong interactions are characterized by three basic properties: asymptotic freedom, confinement and dynamical chiral symmetry breaking.

Owing to the gluonic self-interactions, the QCD coupling becomes smaller at short distances, leading indeed to an asymptotically-free quantum field theory. Perturbation theory can then be applied at large momentum transfers. The resulting predictions have achieved a remarkable success, explaining a wide range of phenomena in terms of a single coupling. The running of α_s has been experimentally tested at different energy scales, confirming the predicted QCD behaviour.

The growing of the running coupling at low-energies makes very plausible that the QCD dynamics generates the required confinement of quarks and gluons into colour-singlet hadronic states. A rigorous proof of this property is, however, still lacking. At present, the dynamical details of hadronization are completely unknown.

Non-perturbative tools, such as QCD sum rules and lattice calculations, provide indirect evidence that QCD also implies the proper pattern of chiral symmetry breaking. The results obtained so far support the existence of a non-zero q-$\bar{q}$ condensate in the QCD vacuum, which dynamically breaks the chiral symmetry of the Lagrangian. However, a formal understanding of this phenomena has only been achieved in some approximate limits.

Thus, we have at present an overwhelming experimental and theoretical evidence that the $SU(3)_C$ gauge theory correctly describes the hadronic world. This makes QCD the established theory of the strong interactions. Nevertheless, the non-perturbative nature of its low-energy limit is still challenging our theoretical capabilities.

APPENDIX A: $SU(N)$ ALGEBRA

$SU(N)$ is the group of $N \times N$ unitary matrices, $UU^\dagger = U^\dagger U = 1$, with $\det U = 1$. The generators of the $SU(N)$ algebra, T^a ($a = 1, 2, \ldots, N^2 - 1$), are hermitian, traceless matrices satisfying the commutation relations

$$[T^a, T^b] = i f^{abc} T^c , \qquad (A.1)$$

the structure constants f^{abc} being real and totally antisymmetric.

The fundamental representation $T^a = \lambda^a / 2$ is N-dimensional. For $N = 2$, λ^a are the usual Pauli matrices, while for $N = 3$, they correspond to the eight Gell-Mann matrices:

$$\lambda^1 = \begin{pmatrix} 0 & 1 & 0 \\ 1 & 0 & 0 \\ 0 & 0 & 0 \end{pmatrix}, \quad \lambda^2 = \begin{pmatrix} 0 & -i & 0 \\ i & 0 & 0 \\ 0 & 0 & 0 \end{pmatrix}, \quad \lambda^3 = \begin{pmatrix} 1 & 0 & 0 \\ 0 & -1 & 0 \\ 0 & 0 & 0 \end{pmatrix}, \quad \lambda^4 = \begin{pmatrix} 0 & 0 & 1 \\ 0 & 0 & 0 \\ 1 & 0 & 0 \end{pmatrix},$$

$$(A.2)$$

$$\lambda^5 = \begin{pmatrix} 0 & 0 & -i \\ 0 & 0 & 0 \\ i & 0 & 0 \end{pmatrix}, \quad \lambda^6 = \begin{pmatrix} 0 & 0 & 0 \\ 0 & 0 & 1 \\ 0 & 1 & 0 \end{pmatrix}, \quad \lambda^7 = \begin{pmatrix} 0 & 0 & 0 \\ 0 & 0 & -i \\ 0 & i & 0 \end{pmatrix}, \quad \lambda^8 = \frac{1}{\sqrt{3}} \begin{pmatrix} 1 & 0 & 0 \\ 0 & 1 & 0 \\ 0 & 0 & -2 \end{pmatrix}.$$

They satisfy the anticommutation relation

$$\{\lambda^a, \lambda^b\} = \frac{4}{N} \delta^{ab} I_N + 2 d^{abc} \lambda^c , \qquad (A.3)$$

where I_N denotes the N-dimensional unit matrix and the constants d^{abc} are totally symmetric in the three indices.

For $SU(3)$, the only non-zero (up to permutations) f^{abc} and d^{abc} constants are

$$\frac{1}{2} f^{123} = f^{147} = -f^{156} = f^{246} = f^{257} = f^{345} = -f^{367} = \frac{1}{\sqrt{3}} f^{458} = \frac{1}{\sqrt{3}} f^{678} = \frac{1}{2} ,$$

$$d^{146} = d^{157} = -d^{247} = d^{256} = d^{344} = d^{355} = -d^{366} = -d^{377} = \frac{1}{2} , \qquad (A.4)$$

$$d^{118} = d^{228} = d^{338} = -2d^{448} = -2d^{558} = -2d^{688} = -2d^{788} = -d^{888} = \frac{1}{\sqrt{3}} .$$

The adjoint representation of the $SU(N)$ group is given by the $(N^2 - 1) \times (N^2 - 1)$ matrices $(T_A^a)_{bc} \equiv -i f^{abc}$. The relations

$$Tr\left(\lambda^a \lambda^b\right) = 4 T_F \delta_{ab} , \qquad\qquad T_F = \frac{1}{2} ,$$

$$(\lambda^a \lambda^a)_{\alpha\beta} = 4 C_F \delta_{\alpha\beta} , \qquad\qquad C_F = \frac{N^2 - 1}{2N} , \qquad (A.5)$$

$$Tr(T_A^a T_A^b) = f^{acd} f^{bcd} = C_A \delta_{ab} , \qquad C_A = N ,$$

define the $SU(N)$ invariants T_F, C_F and C_A. Other useful properties are:

$$(\lambda^a)_{\alpha\delta} (\lambda^a)_{\gamma\delta} = 2 \delta_{\alpha\delta} \delta_{\beta\gamma} - \frac{2}{N} \delta_{\alpha\beta} \delta_{\gamma\delta} ; \qquad Tr\left(\lambda^a \lambda^b \lambda^c\right) = 2 (d^{abc} + i f^{abc}) ;$$

$$Tr(T_A^a T_A^b T_A^c) = i \frac{N}{2} f^{abc} ; \qquad \sum_b d^{abb} = 0 ; \qquad d^{abc} d^{ebc} = \left(N - \frac{4}{N}\right) \delta_{ae} ; \qquad (A.6)$$

$$f^{abe} f^{cde} + f^{ace} f^{dbe} + f^{ade} f^{bce} = 0 ; \qquad f^{abe} d^{cde} + f^{ace} d^{dbe} + f^{ade} d^{bce} = 0 .$$

APPENDIX B: GAUGE-FIXING AND GHOST FIELDS

The fields G_a^μ have 4 Lorentz degrees of freedom, while a massless spin-1 gluon has 2 physical polarizations only. Although gauge invariance makes the additional degrees of freedom irrelevant, they give rise to some technical complications when quantizing the gauge fields.

The canonical momentum associated with G_a^μ, $\Pi_\mu^a(x) \equiv \delta\mathcal{L}_{\rm QCD}/\delta(\partial_0 G_a^\mu) = G_{\mu 0}^a$, vanishes identically for $\mu = 0$. The standard commutation relation

$$[G_a^\mu(x), \Pi_b^\nu(y)]\,\delta(x^0 - y^0) = ig^{\mu\nu}\delta^{(4)}(x - y)\,, \tag{B.1}$$

is then meaningless for $\mu = \nu = 0$. In fact, the field G_a^0 is just a classical quantity, since it commutes with all the other fields. This is not surprising, since we know that there are 2 unphysical components of the gluon field, which should not be quantized. Thus, we could just impose two gauge conditions, such as $G_a^0 = 0$ and $\vec{\nabla}\vec{G}_a = 0$, to eliminate the 2 redundant degrees of freedom, and proceed working with the physical gluon polarizations only. However, this is a (Lorentz) non-covariant procedure, which leads to a very awkward formalism. Instead, one can impose a Lorentz-invariant gauge condition, such as $\partial_\mu G_a^\mu = 0$. The simplest way to implement this is to add to the Lagrangian the gauge-fixing term

$$\mathcal{L}_{\rm GF} = -\frac{1}{2\xi}\left(\partial^\mu G_\mu^a\right)\left(\partial_\nu G_a^\nu\right) \tag{B.2}$$

where ξ is the so-called gauge parameter. The 4 Lorentz components of the canonical momentum

$$\Pi_\mu^a(x) \equiv \frac{\delta\mathcal{L}_{\rm QCD}}{\delta(\partial_0 G_a^\mu)} = G_{\mu 0}^a - \frac{1}{\xi}\,g_{\mu 0}\left(\partial^\nu G_\nu^a\right) \tag{B.3}$$

are then non-zero, and one can develop a covariant quantization formalism. Since (B.2) is a quadratic G_a^μ term, it modifies the gluon propagator:

$$\langle 0|T[G_a^\mu(x)G_b^\nu(y)]|0\rangle = i\delta_{ab}\int\frac{d^4k}{(2\pi)^4}\frac{e^{-ik(x-y)}}{k^2 + i\varepsilon}\left\{-g^{\mu\nu} + (1-\xi)\frac{k^\mu k^\nu}{k^2 + i\varepsilon}\right\}\,. \tag{B.4}$$

Notice, that the propagator is not defined for $\xi = \infty$, i.e. in the absence of the gauge-fixing term (B.2).

In QED, this gauge-fixing procedure is enough for making a consistent quantization of the theory. The initial gauge symmetry of the Lagrangian guarantees that the redundant photon polarizations do not generate non-physical contributions to the scattering amplitudes, and the final results are independent of the arbitrary gauge parameter ξ. In non-abelian gauge theories, like QCD, a second problem still remains.

Let us consider the scattering process $q\bar{q} \rightarrow GG$, which proceeds through the three Feynman graphs shown in Fig. 30. The scattering amplitude has the general form $T = J^{\mu\mu'}\varepsilon_\mu^{(\lambda)}\varepsilon_{\mu'}^{(\lambda')}$. The probability associated with the scattering process

$$\mathcal{P} \sim \frac{1}{2}J^{\mu\mu'}(J^{\nu\nu'})^\dagger\sum_\lambda\varepsilon_\mu^{(\lambda)}\varepsilon_\nu^{(\lambda)*}\sum_{\lambda'}\varepsilon_{\mu'}^{(\lambda')}\varepsilon_{\nu'}^{(\lambda')*} \tag{B.5}$$

involves a sum over the final gluon polarizations. One can easily check that the physical probability $\mathcal{P}_T$, where only the two transverse gluon polarizations are considered in the
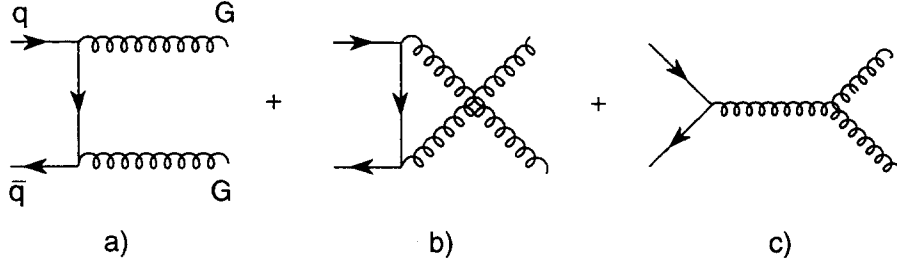
Figure 30: Tree-level Feynman diagrams contributing to $q\bar{q} \to GG$.

sum, is different from the covariant quantity $\mathcal{P}_C$, which includes a sum over all polarization components: $\mathcal{P}_C > \mathcal{P}_T$. In principle, this is not a problem because only $\mathcal{P}_T$ has physical meaning; we should just sum over the physical transverse polarizations to get the right answer. However, the problem comes back at higher orders.
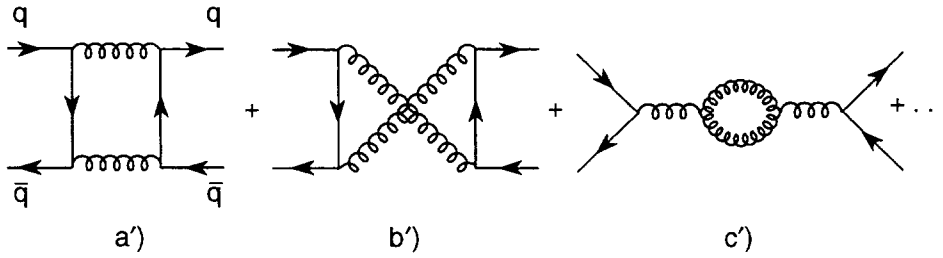

Figure 31: 1-loop diagrams contributing to $q\bar{q} \to q\bar{q}$.

The covariant gluon propagator (B.4) contains the 4 polarization components; therefore higher-order graphs such as the ones in Fig. 31 get unphysical contributions from the longitudinal and scalar gluon polarizations propagating along the internal gluon lines. The absorptive part of these 1-loop graphs (i.e. the imaginary part obtained putting on-shell the two gluon lines within the loop) is equal to $|T(q\bar{q} \to GG)|^2$. Thus, these loops suffer the same probability problem than the tree-level $q\bar{q} \to GG$ amplitude. The propagation of unphysical gluon components implies then a violation of unitarity (the two fake polarizations contribute a positive probability).

In QED this problem does not appear because the gauge-fixing condition $\partial^\mu A_\mu = 0$ still leaves a residual gauge invariance under transformations satisfying $\Box\theta = 0$. This guarantees that (even after adding the gauge-fixing term) the electromagnetic current is conserved, i.e. $\partial_\mu J^\mu_{\text{em}} = \partial_\mu(eQ\bar{\Psi}\gamma^\mu\Psi) = 0$. If one considers the $e^+e^- \to \gamma\gamma$ process, which proceeds through diagrams identical to a) and b) in Fig. 30, current conservation implies $k_\mu J^{\mu\mu'} = k'_{\mu'}J^{\mu\mu'} = 0$, where k_μ and $k'_{\mu'}$ are the momenta of the photons with polarizations λ and λ', respectively (remember that the interacting vertices contained in $J^{\mu\mu'}$ are in fact the corresponding electromagnetic currents). As a consequence, the contributions from the scalar and longitudinal photon polarizations vanish and, therefore, $\mathcal{P}_C = \mathcal{P}_T$.

The reason why $\mathcal{P}_C \neq \mathcal{P}_T$ in QCD stems from the third diagram in Fig. 30, involving a gluon self-interaction. Owing to the non-abelian character of the $SU(3)$ group, the gauge-fixing condition $\partial_\mu G^\mu_a = 0$ does not leave any residual invariance[5]. Thus, $k_\mu J^{\mu\mu'} \neq 0$.

---

5) To maintain $\partial_\mu(G^\mu_a)' = 0$ after the gauge transformation (3.8), one would need $\Box\delta\theta_a = g_s f^{abc}\partial_\mu(\delta\theta_b)G^\mu_c$, which is not possible because G^μ_c is a quantum field.
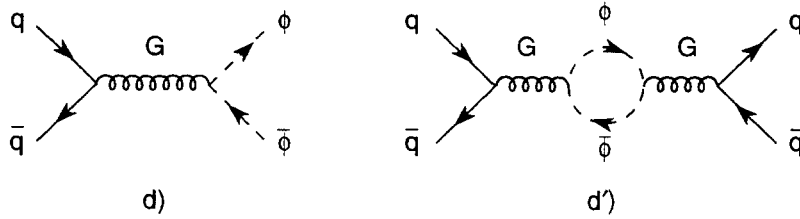
Figure 32: Feynman diagrams involving the ghosts.

Again, the problem could be solved adopting a non-covariant quantization where only the physical transverse polarizations propagate; but the resulting formalism would be awful and very inconvenient for performing practical calculations. A more clever solution consist [60] in adding additional unphysical fields, the so-called *ghosts*, with a coupling to the gluons such that exactly cancels *all* unphysical contributions from the scalar and longitudinal gluon polarizations. Since a positive fake probability has to be cancelled, one needs fields obeying the wrong statistics (i.e. of negative norm) and thus giving negative probabilities. The magic cancellation is achieved by adding to the Lagrangian the Faddeev–Popov term [61],

$$\mathcal{L}_{\mathbf{FP}} = -\partial_\mu \bar{\phi}_a D^\mu \phi^a , \qquad D^\mu \phi^a \equiv \partial^\mu \phi^a - g_s f^{abc} \phi^b G_c^\mu , \qquad (B.6)$$

where $\bar{\phi}^a$, ϕ^a ($a = 1, \ldots, N_C^2 - 1$) is a set of anticommuting (i.e. obeying the Fermi-Dirac statistics), massless, hermitian, scalar fields. The covariant derivative $D^\mu \phi^a$ contains the needed coupling to the gluon field. One can easily check that diagrams d) and d') in Fig. 32 exactly cancel the unphysical contributions from diagrams c) and c') of Figs. 30 and 31, respectively; so that finally $\mathcal{P}_C = \mathcal{P}_T$. Notice, that the Lagrangian (B.6) is necessarily not Hermitian, because one needs to introduce an explicit violation of unitarity to cancel the unphysical probabilities and restore the unitarity of the final scattering amplitudes.

The exact mechanism giving rise to the $\mathcal{L}_{\mathbf{FP}}$ term can only be understood (in a simple way) using the more powerful path-integral formalism, which is beyond the scope of these lectures. The only point I would like to emphasize here, is that the addition of the gauge-fixing and Faddeev–Popov Lagrangians is just a mathematical trick, which allows to develop a simple covariant formalism, and therefore a set of simple Feynman rules, making easier to perform explicit calculations.

REFERENCES

[1] I.J.R. Aitchison and A.J.G. Hey, *Gauge Theories in Particle Physics*, Graduate Student Series in Physics (IOP Publishing Ltd, Bristol, 1989).

[2] T. Muta, *Foundations of Quantum Chromodynamics*, Lecture Notes in Physics – Vol. 5 (World Scientific, Singapore, 1987).

[3] P. Pascual and R. Tarrach, *QCD: Renormalization for the Practitioner* (Springer–Verlag, Berlin, 1984).

[4] F.J. Yndurain, *The Theory of Quark and Gluon Interactions*, Texts and Monographs in Physics (Springer-Verlag, New York, 1993).

[5] T. Hebbeker, Phys. Rep. 217 (1992) 69.

[6] D. Espriu, *Perturbative QCD*, Proc. XXII Int. Meeting on Fundamental Physics (Jaca, 1994), Univ. Barcelona preprint UB-ECM-PF-94/24;
J. Fuster, *Recent Results on QCD at LEP*, Proc. XXII Int. Meeting on Fundamental Physics (Jaca, 1994).

[7] S. Bethke, *Summary of α_s Measurements*, in Proc. QCD94 Workshop (Montpellier, July, 1994), ed. S. Narison, Nucl. Phys. B (Proc. Suppl.) 39B,C (1995) 198.

[8] B.R. Webber, *QCD and Jet Physics*, Proc. XXVII Int. Conf. on High Energy Physics (Glasgow, July 1994), eds. P.J. Bussey and I.G. Knowles (IOP, Bristol, 1995), Vol. I, p. 213.

[9] M. Schmelling, *QCD Results from the Study of Hadronic Z-Decays*, CERN-PPE/94-184.

[10] Particle Data Group, *Review of Particle Properties*, Phys. Rev. D50 (1994) 1173.

[11] M. Gell-Mann, Phys. Lett. 8 (1964) 214;
G. Zweig, CERN preprints CERN-TH 401 and 412 (1964), unpublished.

[12] M. Gell-Mann, Acta Phys. Austriaca Suppl. 9 (1972) 733;
M. Han and Y. Nambu, Phys. Rev. 139B (1965) 1006.

[13] S.L. Adler and W.A. Bardeen, Phys. Rev. 182 (1969) 1517.

[14] J.D. Bjorken, Phys. Rev. 179 (1969) 1547.

[15] C.J. Callan and D.J. Gross, Phys. Rev. Lett. 22 (1969) 156.

[16] W.B. Attwood, in Proc. 1979 SLAC Summer Institute on Particle Physics (SLAC-224, 1980), ed. A. Mosher, Vol. 3.

[17] D.H. Perkins, *Introduction to High Energy Physics* (Addison–Wesley, Menlo Park, 1980) 3rd edition.

[18] H. Fritzsch and M. Gell-Mann, Proc. XVI Int. Conf. on High Energy Physics, eds. J.D. Jackson and A. Roberts (Fermilab, 1972), Vol. 2, p. 135;
H. Fritzsch, M. Gell-Mann and H. Leutwyler, Phys. Lett. 47B (1973) 365.

[19] T. Kinoshita (editor), *Quantum Electrodynamics*, Advanced Series on Directions in High Energy Physics, Vol. 7 (World Scientific, Singapore, 1990);
T. Kinoshita, Phys. Rev. D47 (1993) 5013.

[20] G. t'Hooft, Nucl. Phys. B61 (1973) 455.

[21] W.A. Bardeen, A.J. Buras, D.W. Duke and T. Muta, Phys. Rev. D18 (1978) 3998.

[22] D.J. Gross and F. Wilczek, Phys. Rev. Lett. 30 (1973) 1343.

[23] H.D. Politzer, Phys. Rev. Lett. 30 (1973) 1346.

[24] S. Coleman and D.J. Gross, Phys. Rev. Lett. 31 (1973) 851.

[25] W.E. Caswell, Phys. Rev. Lett. 33 (1974) 244;
D.R.T. Jones, Nucl. Phys. B75 (1974) 531;
O.V. Tarasov, A.A. Vladimirov and A. Yu. Zharkov, Phys. Lett. 93B (1980) 429.

[26] K.G. Chetyrkin, A.L. Kataev and F.V. Tkachov, Phys. Lett. 85B (1979) 277;
M. Dine and J. Sapirstein, Phys. Rev. Lett. 43 (1979) 668;
W. Celmaster and R. Gonsalves, Phys. Rev. Lett. 44 (1980) 560.

[27] S.G. Gorishny, A.L. Kataev and S.A. Larin, Phys. Lett. B259 (1991) 144;
L.R. Surguladze and M.A. Samuel, Phys. Rev. Lett. 66 (1991) 560.

[28] D. Haidt, in *Precision Tests of The Standard Electroweak Model*, ed. P. Langacker, Directions in High Energy Physics Vol. 14 (World Scientific, 1993).

[29] R. Barbieri, these proceedings.

[30] A. Pich, *The Standard Model of Electroweak Interactions*, Lectures at the CERN Academic Training (Geneva, November 1993) and at the XXII Int. Winter Meeting on Fundamental Physics (Jaca, February 1994), Univ. Valencia preprint FTUV/94-62 [hep-ph/9412274].

[31] The LEP Collab. and the LEP Electroweak Working Group, CERN/PPE/94-187.

[32] E. Braaten, Phys. Rev. Lett. 60 (1988) 1606; Phys. Rev. D39 (1989) 1458.

[33] S. Narison and A. Pich, Phys. Lett. B211 (1988) 183.

[34] E. Braaten, S. Narison and A. Pich, Nucl. Phys. B373 (1992) 581.

[35] F. Le Diberder and A. Pich, Phys. Lett. B286 (1992) 147.

[36] A. Pich, *QCD Predictions for the τ Hadronic Width: Determination of $\alpha_s(m_\tau^2)$*, in Proc. QCD94 Workshop (Montpellier, July, 1994), ed. S. Narison, Nucl. Phys. B (Proc. Suppl.) 39B,C (1995) 326.

[37] F. Le Diberder and A. Pich, Phys. Lett. B289 (1992) 165.

[38] D. Buskulic et al. (ALEPH), Phys. Lett. B307 (1993) 209.

[39] F. Bloch and A. Nordsieck, Phys. Rev. 52 (1937) 54.

[40] T. Kinoshita, J. Math. Phys. 3 (1962) 650;
T.D. Lee and M. Nauenberg, Phys. Rev. 133B (1964) 1549.

[41] W. Bartel et al. (JADE), Z. Phys. C33 (1986) 23; Phys. Lett. B213 (1988) 235.

[42] S. Catani et al., Phys. Lett. B263 (1991) 491; B269 (1991) 432; B272 (1991) 368.

[43] S. Bethke, *Jets in Z^0 Decays*, Proc. *QCD 20 Years Later* (Aachen, 1992), eds. P.M. Zerwas and H.A. Kastrup (World Scientific, Singapore, 1993), Vol. 1, p.43.

[44] R. Akers et al. (OPAL), Z. Phys. C65 (1995) 367.

[45] K. Gottfried, Phys. Rev. Lett. 18 (1967) 1154.

[46] L.N. Lipatov, Sov. J. Nucl. Phys. 20 (1975) 94;
V.N. Gribov and L.N. Lipatov, Sov. J. Nucl. Phys. 15 (1972) 438.

[47] G. Altarelli and G. Parisi, Nucl. Phys. B126 (1977) 298.

[48] K. Wilson, Phys. Rev. 179 (1969) 1499.

[49] T. Ahmed et al. (H1), DESY 95-006 [hep-ex/9503001]; Nucl. Phys. B407 (1993) 515.

[50] M. Derrick et al. (ZEUS), Z. Phys. C65 (1995) 379; Phys. Lett. B316 (1993) 412.

[51] P. Amaudruz et al. (NMC), Phys. Lett. B259 (1992) 159.

[52] A.C. Benvenuti et al. (BCDMS), Phys. Lett. B237 (1990) 592.

[53] A.D. Martin, W.J. Stirling and R.G. Roberts, Rutherford preprint RAL-95-021 [hep-ph/9502336].

[54] M. Virchaux and A. Milsztajn, Phys. Lett. B274 (1992) 221.

[55] S. Coleman, J. Math. Phys. 7 (1966) 787.

[56] J. Goldstone, Nuov. Cim. 19 (1961) 154.

[57] S. Weinberg, Phys. Rev. Lett. 17 (1966) 616.

[58] A. Pich, *Chiral Perturbation Theory*, Rep. Prog. Phys. 58 (1995) (to appear) [hep-ph/9502366].

[59] S. Adler and R.F. Dashen, *Current Algebras*, (Benjamin, New York, 1968);
V. de Alfaro, S. Fubini, G. Furlan and C. Rossetti, *Currents in Hadron Physics*, (North-Holland, Amsterdam, 1973).

[60] R.P. Feynman, Acta Phys. Polonica 24 (1963) 697.

[61] L.D. Faddeev and Y.N. Popov, Phys. Lett. 25B (1967) 29.